

A FAST, 3 MV MARX GENERATOR FOR MEGAVOLT OIL SWITCH
TESTING AND INTEGRATED ABRAMYAN NETWORK DESIGN

A Thesis

Presented to

The Faculty of the Graduate School

University of Missouri-Columbia

In Partial Fulfillment

Of the Requirements for the Degree

Master of Science

by

LAURA K. HEFFERNAN

Dr. Randy Curry, Thesis Supervisor

DECEMBER 2005

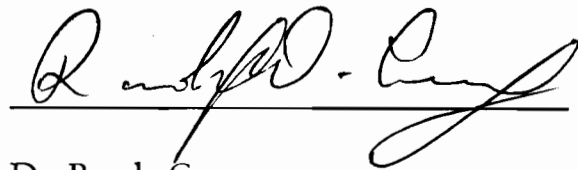
The undersigned, appointed by the Dean of the Graduate School, have
examined the thesis entitled

A FAST, 3 MV MARX GENERATOR FOR MEGAVOLT OIL SWITCH
TESTING AND INTEGRATED ABRAMYAN NETWORK DESIGN

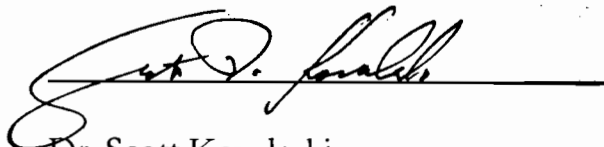
presented by Laura Heffernan

a candidate for the degree of Master of Science

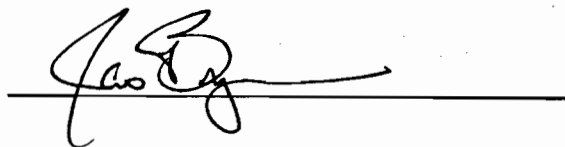
and hereby certify that in their opinion it is worthy of acceptance.



Dr. Randy Curry



Dr. Scott Kovaleski



Dr. James Bryan

ACKNOWLEDGEMENTS

I would like to thank my advisor, Dr. Curry, for his guidance throughout this research and Dr. Kovalski and Dr. Bryan for their collaboration. I would also like to thank all those that assisted me in the many facets of this project including Dr. McDonald, Peter Norgard, Mark Nichols, Josh Leckbee, Keith LeChien, Scott Castagno, and the many undergraduate assistants. A special thanks goes to Mom, Dad, Mary, Brian, and Paul for their support and to Tim for his constant encouragement.

TABLE OF CONTENTS

ACKNOWLEDGEMENTS	ii
INDEX OF FIGURES.....	v
INDEX OF TABLES.....	vi
CHAPTER 1. INTRODUCTION.....	1
1.1. Background	1
1.2. Marx Generators	1
1.3. Abramyan Networks	4
References for Chapter 1	7
CHAPTER 2. DESCRIPTION OF SYSTEM.....	9
2.1. Pulsed Power Research Laboratory	9
2.2. UMC Marx Generator	10
2.3. Charging	15
2.4. Triggering	20
2.5. Control Systems	22
2.6. Peaking Capacitor and Oil Switch	24
References for Chapter 2	29
CHAPTER 3. DIAGNOSTICS.....	31
3.1. Requirements	31
3.2. Voltage Divider Theory	32
3.3. Post-switch Divider	35
3.4. Pre-switch Divider	38
3.5. Calibration	40
References for Chapter 3	45
CHAPTER 4. MODELING OF MARX.....	47
4.1. Marx Circuits	47
4.2. PSPICE Simulations	47
4.3. Breakdown Calculations	49
4.4. Electrostatic Simulations	53
References for Chapter 4	56
CHAPTER 5. SWITCH EXPERIMENTS	57
5.1. Experimental Setup	57
5.2. Experimental Results	60
References for Chapter 5	65
CHAPTER 6. ABRAMYAN NETWORK DESIGN.....	66
6.1. PFNs, PFLs, and the Abramyan Network	66
6.2. Physical Implementation of the Abramyan	69
6.3. Circuit Simulations	72
References for Chapter 6	82
CHAPTER 7. CONCLUSION.....	84
APPENDIX A. SPARK GAP DIMENSIONS	86
APPENDIX B. MARX SIMULATION CODE.....	87

APPENDIX C. MARX OPERATION	91
APPENDIX D. MARX SHOT LOG	93
APPENDIX E. MATLAB CODE	96
APPENDIX F. MATHEMATICA CODE	100
APPENDIX G. ABRAMYAN SIMULATION CODE	103

INDEX OF FIGURES

Figure 1.1. Marx stages.....	2
Figure 1.2. Simple Marx equivalent circuit.....	2
Figure 1.3. Typical output pulse of Marx generator into a purely resistive load.....	3
Figure 1.4. Simple Abramyan circuit.....	5
Figure 1.5. Abramyan circuit signal decomposition.....	5
Figure 2.1. UMC pulsed power lab.....	9
Figure 2.2. Marx circuit.....	11
Figure 2.3. Hydraulic pumping system.....	12
Figure 2.4. Indoor oil containment tank with capacitors in raised position.....	12
Figure 2.5. Secondary oil storage tank.....	13
Figure 2.6. Oil pumping station flow diagram.....	14
Figure 2.7. Dual-polarity charging schematic.....	16
Figure 2.8. Charging and triggering resistors.....	17
Figure 2.9. Ground reference resistors.....	18
Figure 2.10. Spark gaps installed in Marx.....	19
Figure 2.11. Assembled spark gap.....	19
Figure 2.12. Trigger generator.....	20
Figure 2.13. Gas and trigger lines.....	21
Figure 2.14. Crowbar assembly with input charging and triggering lines.....	21
Figure 2.15. Control cabinet.....	22
Figure 2.16. Control system block diagram.....	23
Figure 2.17. Peaking capacitor.....	25
Figure 2.18. Oil switch enhanced electrode.....	26
Figure 2.19. Simplified Marx with peaking capacitor.....	28
Figure 3.1. Voltage divider circuit.....	32
Figure 3.2. Simplified voltage divider implemented in diagnostic circuit.....	33
Figure 3.3. Voltage divider middle electrode.....	34
Figure 3.4. Voltage divider stages.....	35
Figure 3.5. Post-switch voltage divider.....	36
Figure 3.6. Pre-switch voltage divider.....	40
Figure 3.7. Voltage divider calibration configuration.....	41
Figure 3.8. Digital calibration of post-switch divider.....	42
Figure 3.9. Analog calibration of post-switch divider.....	42
Figure 3.10. Digital calibration of pre-switch divider.....	43
Figure 3.11. Diagnostic output connections and Faraday cage.....	44
Figure 4.1. Simplified 30 stage UMC Marx circuit.....	47
Figure 4.2. Simulated Marx output pulse with and without peaker.....	48
Figure 4.3. Two spheres with equal radii.....	50
Figure 4.4. Sphere and plane.....	50
Figure 4.5. Electric field calculations with variable voltage and electrode separation.....	51
Figure 4.6. Field enhancement factor for sphere-sphere and sphere-plane geometries.....	52
Figure 4.7. Electric field strength with varying electrode separation.....	53

Figure 4.8. Electrostatic simulation of output switch field strength before Marx fires.....	54
Figure 4.9. Enlarged view of tip of enhanced electrode electric field strengths	54
Figure 4.10. Electrostatic simulation of output switch potentials before Marx fires	55
Figure 5.1. Marx spark gap operating curve	58
Figure 5.2. Trigger generator operating curve	58
Figure 5.3. Oil peaking switch operating curve	59
Figure 5.4. Marx output data	61
Figure 5.5. Marx simulated output.....	61
Figure 5.6. Data from both pre and post-switch dividers (Shot 8)	63
Figure 5.7. Marx shot with multi-channel arcs to ground (Shot 33)	63
Figure 5.8. Oil breakdown with Hipotronics tester	64
Figure 6.1. Guillemin Type A PFN	67
Figure 6.2. Type A PFN for UMC Marx	68
Figure 6.3. Two cylinders (approximating turns of copper pipe).....	70
Figure 6.4. Equivalent Marx circuit with twenty-two stages	71
Figure 6.5. Basic Abramyan in twenty-two stage Marx.....	71
Figure 6.6. Abramyan network with inductor values 1 μ H - 9 μ H.....	74
Figure 6.7. Varying Abramyan network inductor values	75
Figure 6.8. Signal decomposition of Abramyan with Marx	77
Figure 6.9. Conceptual design of UMC Marx with Abramyan network.....	77
Figure 6.10. Marx and Abramyan with 5 μ H inductor	78
Figure 6.11. Abramyan with damping resistor	79
Figure 6.12. Full length output from Abramyan and Marx.....	79
Figure 6.13. Output pulses with damping resistor in the 5 μ H Abramyan network	80

INDEX OF TABLES

Table 2.1. UMC Marx parameters	10
Table 2.2. CuSO ₄ resistors.....	17
Table 4.1. Pulse characteristics from Marx simulation without peaking circuit.....	49
Table 4.2. Pulse characteristics from Marx simulation with peaking circuit	49
Table 5.1. Output pulse characteristics	60
Table 6.1. Expected pulse lengths from variable inductor values	73
Table 6.2. Abramyan network pulse characteristics, $L_d = 5 \mu$ H	78
Table 6.3. Pulse lengths for resistance values in Abramyan.....	81

CHAPTER 1. INTRODUCTION

1.1. Background

A fundamental component of pulsed power systems is energy storage. The most popular method of energy storage for many applications including high energy density physics, particle accelerators and flash radiography, high power microwave generation, and directed energy defense systems is the Marx generator. This broad application base requires a system that is simple yet robust. In addition to the Marx, pulse-shaping circuits are often required to tune the output for specific load parameters. This thesis will discuss the operation of a typical Marx and include a design to generate a rectangular pulse using a simple circuit addition to the Marx.

1.2. Marx Generators

In 1923, Erwin Marx patented the circuit for a generator with the fundamental principle of charging capacitors in parallel and switching the capacitors in series into a load [1]. The capacitors were charged through resistors and switched using simple two-electrode spark gaps triggered by overvoltage [2], [3]. More recent designs have presented variations, but the concept is much the same [3], [4], [5], [6]. Figure 1.1 shows the first few stages of an ideal Marx generator with a resistive load.

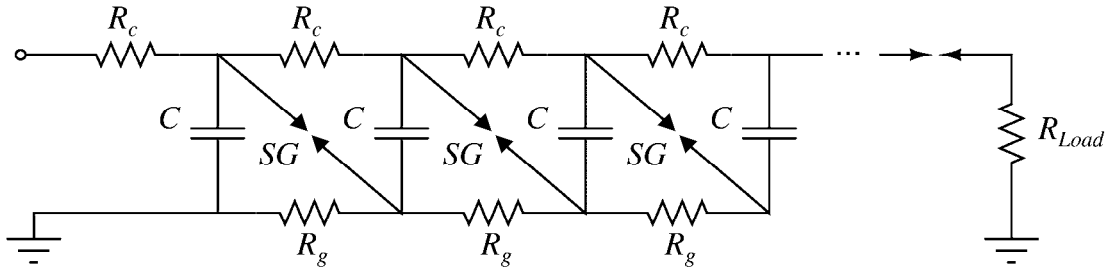


Figure 1.1. Marx stages

The Marx charges its capacitors through the charging resistors, R_c . After reaching the desired voltage, the first spark gap breaks down. Twice the amount of voltage is then seen across the second spark gap. The voltage is too high for that gap to hold off, so it also breaks down. This is repeated for each stage of the Marx and is considered “erecting the Marx”. The Marx can then be converted into an equivalent circuit including a single capacitor discharging, in this example, into a resistive load. The series inductor in the equivalent circuit in Figure 1.2 represents the non-ideal case where [7]:

$$L_{Marx} = L_{switches} + L_{caps} + L_{connections} \quad (1.1)$$

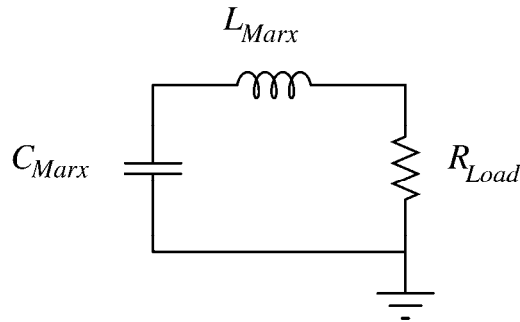


Figure 1.2. Simple Marx equivalent circuit

The simplified erected Marx circuit allows all of the capacitive stages to appear as a single capacitor, C_{Marx} , where N is defined as the number of stages in the Marx.

$$C_{Marx} = \frac{C_{stage}}{N} \quad (1.2)$$

The output voltage, V_{Marx} , of these combined stages, or the output of the Marx, is the product of the number of Marx stages and the charge voltage per stage.

$$V_{Marx} = N \cdot V_{stage} \quad (1.3)$$

The total energy, E_{Marx} , stored in the Marx can also be calculated from the values per stage.

$$E_{Marx} = \frac{1}{2} C_{stage} \cdot V_{stage}^2 \cdot N \quad (1.4)$$

$$E_{Marx} = \frac{1}{2} C_{Marx} \cdot V_{Marx}^2 \quad (1.5)$$

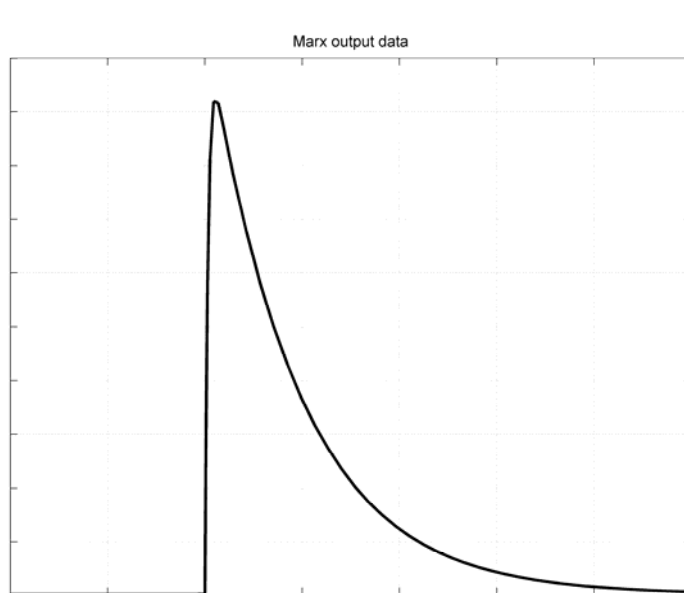


Figure 1.3. Typical output pulse of Marx generator into a purely resistive load

The output of a Marx into a damped resistive load can be expected to appear similar to the plot in Figure 1.3. A capacitive bank ideally switching into a resistive load will result in Equation 1.6. Risetimes, fall times, and pulse widths will vary with parametric value changes, but the result will maintain an exponential RC decay. For the same circuit containing an inductor L , the 10-90 % risetime can be expressed as $2.2 \frac{L}{R}$ [8].

$$V = V_o \cdot e^{-t/RC} \quad (1.6)$$

Although Marx generators can be relatively inexpensive and easy to build, a pulse of this type may not be desirable for many applications. A flat-top pulse is especially valuable for defense systems including high power microwave and directed energy applications. Two of the most commonly used alternatives to increase pulse width include Pulse Forming Lines (PFLs) and Pulse Forming Networks (PFNs). Both of these well-documented approaches have their own sets of advantages and disadvantages [9], [10]. Plans for the University of Missouri-Columbia (UMC) Marx utilize a different approach called an Abramyan network. The eponymous E.A. Abramyan developed this cost-efficient alternative to extending the pulse from a Marx generator into a rectangularly shaped pulse with the addition of a single inductor.

1.3. Abramyan Networks

The basic Marx circuit in Figure 1.2 can be modified to produce a rectangular pulse with the addition of a single component [11]. The Abramyan network “reverse-charges” a fraction of Marx stages and requires placement of an inductor of an optimized value in parallel with those stages [12]. The basic Abramyan network circuit is shown in Figure 1.4. Both C_a and L_a are components already in the Marx. They are simply stages of the Marx that are reverse-charged,

or oppositely charged from the other “normally-charged” stages. The inductance L_a is the series inductance of those stages and not an actual physical inductor. The only addition to the Marx circuit is L_d . This inductor is optimized to form a ringing circuit, or tank circuit, that oscillates to extend and ‘flatten’ the output pulse of the Marx. Taking the Laplace transform of the circuit and plotting its signal components, as in Figure 1.5, emphasizes the importance of the ringing portion of the circuit.

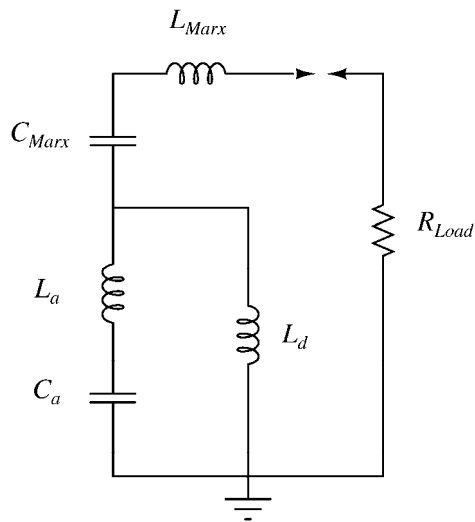


Figure 1.4. Simple Abramyan circuit

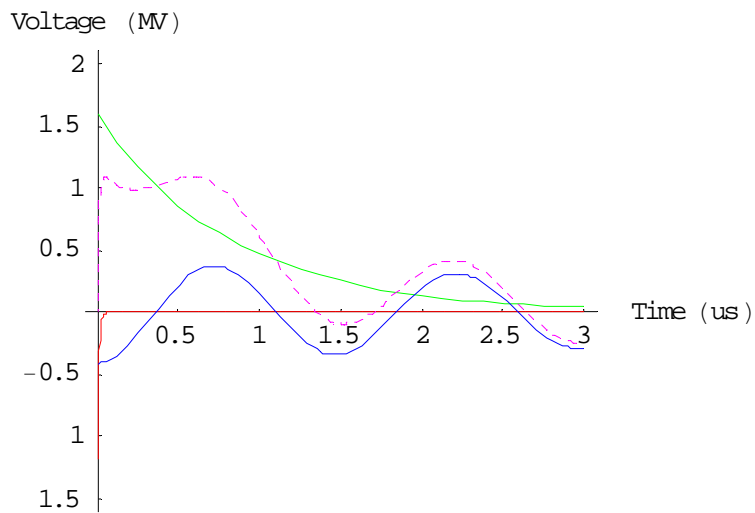


Figure 1.5. Abramyan circuit signal decomposition

In Figure 1.5, the green line is the main normally-charged capacitors' decay. The red line represents the reverse-charged capacitors' decay. The blue line represents the ringing of the Abramyan network section of the Marx. These three components combine to form the output pulse of the Marx (dashed purple line). As can be easily seen, the pulse width is greatly increased from its original form without the Abramyan network addition. The full Mathematica code for this signal decomposition can be found in Appendix F. The design of this circuit for the UMC Marx will be discussed in detail in Chapter 6.

References for Chapter 1

- [1] E. Marx, “Verfahren zur Schlagprüfung von Isolatoren und anderen elektrischen Vorrichtungen”, *Deutsches Reich Reichspatentamt Patentschrift 455933*, Oct. 1923.
- [2] J. F. Francis, “High voltage pulse techniques”, Texas Tech University, 1976.
- [3] R. A. Fitch, “Marx – and Marx-like – high-voltage generators”, *IEEE Transactions on Nuclear Science*, vol. 18, no. 4, pp. 190-198, Aug. 1974.
- [4] K. R. Prestwich and D. L. Johnson, “Development of an 18-megavolt Marx generator”, *IEEE Transactions on Nuclear Science*, vol. 16, no. 3, pp. 64-69, Jun. 1969.
- [5] J. D. Graham, D. G. Gale, W. E. Sommars, and S. E. Calico, “Compact 400 kV Marx generator with common switch housing,” *Proceedings of 11th IEEE Pulsed Power Conference*, 1997.
- [6] F. E. Peterkin, D. C. Stoudt, B. J. Hankla, K. A. Boulais, J. S. Bernardes, “Performance characteristics of a 1 MV miniature Marx bank”, *Proceedings of the 12th IEEE Pulsed Power Conference*, 1999.
- [7] R. J. Adler, “Pulse power formulary,” North Star Research Corporation, [Online]. Available: <http://www.northstar-research.com/PDF/Formweb1.pdf>
- [8] G. A. Mesyats, *Pulsed Power*, Plenum, 2005.
- [9] G. N. Glasoe and J. V. Lebacqz, Eds., “Pulse Generators”, *Massachusetts Institute of Technology Radiation Laboratory Series*, McGraw-Hill, 1948.
- [10] P. W. Smith, *Transient Electronics: Pulsed Circuit Technology*, Wiley, 2002.
- [11] R. Curry, K. Nielsen, I. Smith, “Abramyan networks: a general purpose network for linear induction accelerators”, Pulse Sciences, Inc., San Leandro, CA, Apr. 1986

- [12] E. A. Abramyan, E. N. Efimov, and G. D. Kuleshov, "Correction of the pulse shape of an Arkad'ev-Marks voltage generator," High-Temperature Institute of the Academy of Sciences of the USSR, Moscow. Translated from *Pribory i Tekhnika Éksperimenta*, No. 4, pp.170-172, Jul.-Aug. 1979.

CHAPTER 2. DESCRIPTION OF SYSTEM

2.1. Pulsed Power Research Laboratory



Figure 2.1. UMC pulsed power lab

The UMC Marx and all its subsystems are housed in the Pulsed Power Research Laboratory on campus. This lab enables students to design, build, and test large-scale pulsed power projects. One of the goals of the lab was to develop a test facility to study oil breakdown of enhanced and uniform gaps. The now operational test facility includes a thirty-stage, three-megavolt Marx generator. The pulser is designed to deliver a 3 MV output pulse with a risetime (10-90%) of ≤ 10 ns with a peaking gap. The output polarity of the pulser can be easily reversed for switch and dielectric testing. The configurations tested include large electrode gap spacings with point-ball electrodes. This chapter will describe the system configuration and components required for the test facility. Test results from these experiments will be reported in Chapter 5.

Chapter 6 will discuss a conceptual design for a simple modification which will allow a rectangular pulse to be applied to the sample under test.

2.2. UMC Marx Generator

The UMC Marx generator has a total capacitance of 1.6 nF with a series inductance of 4.6 μ H [1]. At full charge, the Marx switches 7.2 kJ into the current 300 Ω dummy load. The Marx is modular in design with the capability for removal or addition of stages to increase or decrease capacitance. Two capacitors can be added per half stage for a total erected capacitance of 2.75 nF at 3 MV. The current Marx values are listed in Table 2.1 and the circuit is shown in Figure 2.2.

Table 2.1. UMC Marx parameters

Number of stages	30
Stage charge voltage	100 kV
Stage capacitance	48 nF
Total capacitance	1.6 nF
Series inductance	4.6 μ H

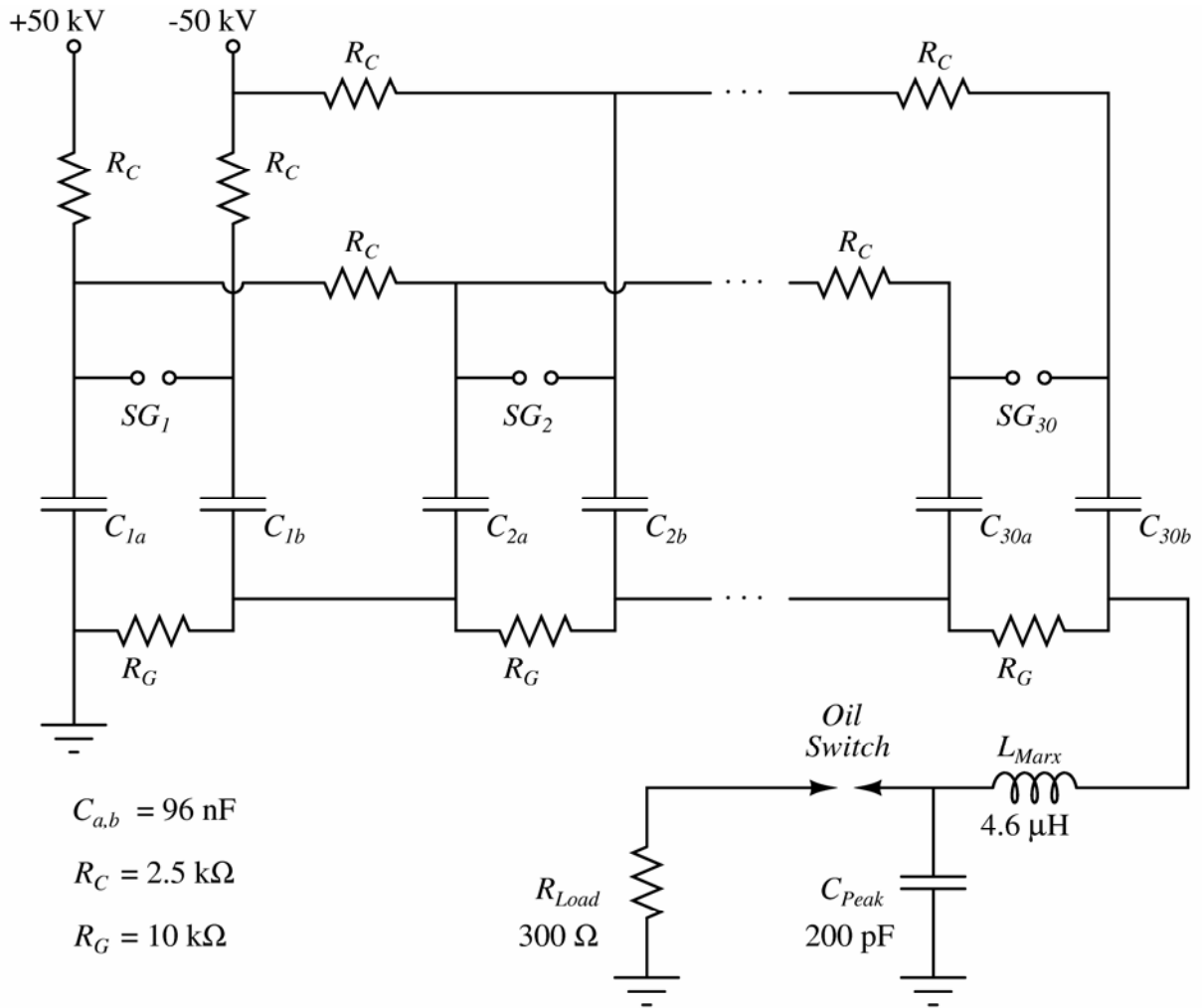


Figure 2.2. Marx circuit

The Marx generator's capacitors, resistors, and switches are supported by a nylon backbone suspended below a steel ground plane. This frame can be raised to expose the capacitors, resistors, and switches via a hydraulic lift system shown in Figure 2.3. The hydraulic pumping system is positioned near the Marx and is responsible for pressurizing the four cylinders that raise and lower the frame.



Figure 2.3. Hydraulic pumping system



Figure 2.4. Indoor oil containment tank with capacitors in raised position

During operation, the Marx is immersed in the indoor oil containment tank shown in Figure 2.4. It is approximately 15 ft long, 3.5 ft wide, and 5 ft deep with a cylindrical oil-filled extension at the high voltage end of the tank. The tank holds approximately 2,000 gallons of Shell Diala AX transformer oil with the capacitors, resistors, switches, and support system submerged [2]. The steel tank has been painted with International 850 Interline tank paint for rust prevention [3].



Figure 2.5. Secondary oil storage tank

The secondary oil storage tank seen in Figure 2.5 is located outside of the building within an additional retaining wall for environmental safety. The tank is used to store the oil during periods of time in which the Marx is not in use. It has a storage capacity of 3,000 gallons and remains unpainted on the inside to reduce impurities in the oil during long-term storage. To

prevent rust due to any outdoor moisture, the interior walls have been completely lubricated with the oil. The outside of the tank has been painted and all openings have been resealed.

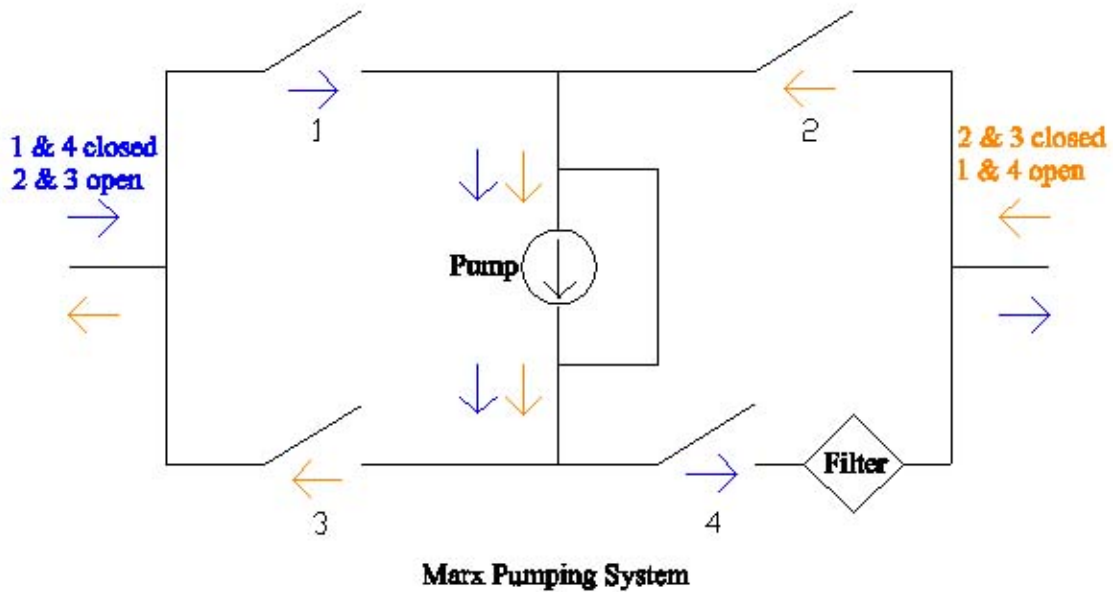


Figure 2.6. Oil pumping station flow diagram

The tank is connected to a pumping station also located within the retaining walls as seen in the forefront of the image in Figure 2.5. The pumping station described in Figure 2.6 contains a Lincoln three-phase motor, 8300 Series Pall filter housing with a 42,326 cm², 3 μ filter [4], and refurbished control box. The control box consists of an Allen-Bradley AN16BN0AC starter and C341BC transformer in a weather-resistant box attached to the pumping and filtering cart frame. Three-phase power is supplied from the building to the control box and pumping motor.

2.3. Charging

The Marx is dual-polarity charged and contains thirty capacitive stages. Each stage consists of six 32 nF tubular capacitors. The six capacitors per stage are arranged three in parallel to form a half-stage with two half-stages in series. The capacitors are members of the Condenser Products KMOP Series [5]. The capacitors are housed in thermo-plastic tubing and consist of a composite dielectric of kraft tissue and polyester film with a mineral oil impregnant. The capacitor voltage maximum is 250 kV with a temperature range of -40°C to +65°C. The capacitors are designed for 500,000 shots with no applied reverse voltage. With applied reverse voltage, the number of shots in the lifetime of the capacitor will decrease according to the formula described in Equation 2.1 given by Condenser Products [6].

$$\text{number of shots} = \left(\frac{-1.57}{\ln(\text{reverse voltage \%})} \right)^{-2.2} \cdot 500,000 \quad (2.1)$$

According to this formula, for a 50% reversal, the capacitor lifetime is 82,000 shots. Similarly, 80% reversal yields 7,000 shots. The Marx is not initially configured for any voltage reversal but possible alterations to the system discussed later in the Abramyan section will prove this equation relevant.

The Marx is designed to be charged with two, ± 50 kV power supplies for a 3 MV output pulse. Currently, the Marx is configured to charge with one +50 kV Glassman power supply and one -40 kV, Kaiser power supply [7], [8]. The +50 kV, Glassman Model PS/WG-50P6, is a 300 W power supply that can deliver 60 mA. The -40 kV Kaiser Series 1000 is a 500 W power supply that can deliver 12.5 mA. Because of this variation in power supply current, the capacitors charge at separate rates and reach their charge voltage at different times. Although not the ideal case, this poses no direct problems for operation of the Marx generator.

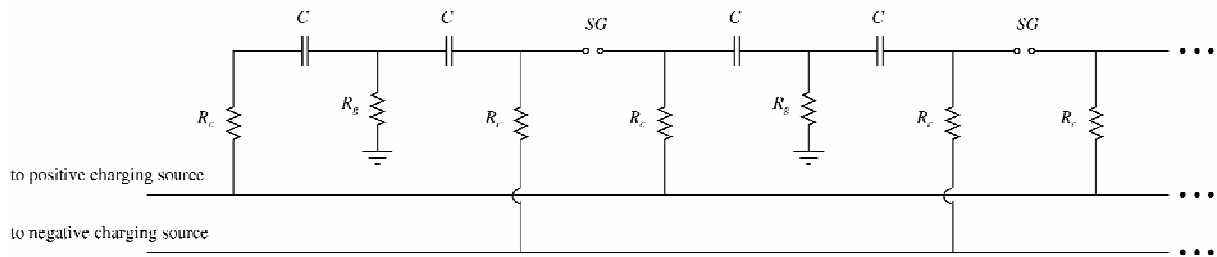


Figure 2.7. Dual-polarity charging schematic

With dual-polarity charging, the number of spark gaps required is reduced by half [9]. In the simple single-polarity Marx charging configuration, a spark gap switch is required for each capacitor. The switch is located between the high voltage end of one capacitor and the low voltage end of the next capacitor. Figure 2.7 demonstrates how including both positive and negative polarity charging in the circuit can eliminate half of the required spark gaps. This charging configuration is utilized in the UMC Marx.

Although the Marx is largely a capacitive bank, many resistors are required for a variety of applications within the pulser. For the UMC Marx, charging, triggering and ground reference resistors were all essential. Values of resistances for these three types are noted in Table 2.2 [1]. Also described in the table are values necessary for constructing these resistors. Because the energy requirements for resistors in the Marx were too high for traditional resistors, liquid resistors were used. Copper sulfate (CuSO_4) is the most commonly used solution for liquid resistors and maintains a dielectric strength of $> 200 \text{ kV/cm}$ [10], [11]. Due to the ease and cost-efficiency of design, liquid resistors were constructed for the UMC Marx with bead-blasted copper electrodes, Tygon B-44-3 beverage tubing [12], 2-ear Oetiker clamps, deionized and

degassed water, and crystalline copper sulfate pentahydrate. Images of the charging, triggering, and ground reference resistors are seen in Figure 2.8 and Figure 2.9.

Table 2.2. CuSO₄ resistors [1]

Description	Quantity	Resistance (Ω)	Inner Diameter (in)	Length (in)	Volume Resistivity (Ω/cm)	Solution (gm/L)
Charging	62	2.5 k	0.5	13.75	91	38
Trigger	30	1.5 k	0.5	11.75	67	63
GND Ref	30	10 k	0.5	9.25	540	4



Figure 2.8. Charging and triggering resistors



Figure 2.9. Ground reference resistors

The spark gap switches installed in the UMC Marx (Figure 2.10) are similar in configuration to the original simple two-electrode switches in early circuits [13]. They are very similar in operation to the Series T-670 spark gap switches currently produced by Titan Corporation Pulse Sciences Division [14]. Autocad drawings of the UMC Marx spark gap dimensions are shown in Appendix A. The acrylic switch housing contains two brass electrodes with a mid-plane for triggering. An image of a fully assembled switch can be seen in Figure 2.11

The switches are pressurized with sulfur hexafluoride (SF_6) during operation of the Marx. The use of SF_6 enables the spark gaps to be operated at lower pressures than synthetic air would allow. The switches will function with air, but at much higher pressures for comparable voltage hold-off. The SF_6 gas lines are attached at the top of the switches and are connected in

series to all 30 gaps. Swagelok fittings connect the segments of Dayco Nylo-Seal tubing between the switches for filling and purging the SF₆ between sets of shots.



Figure 2.10. Spark gaps installed in Marx

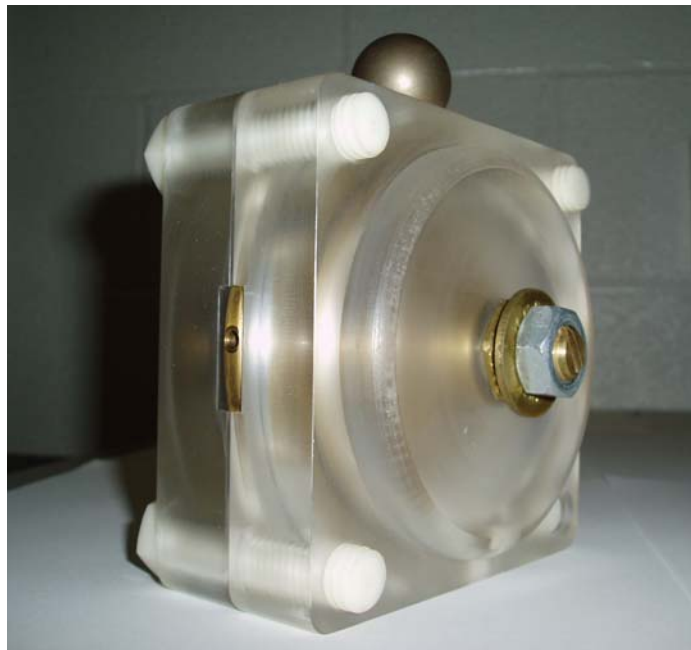


Figure 2.11. Assembled spark gap

2.4. Triggering

The Marx is triggered by the pulsed trigger system in Figure 2.12 consisting of a high voltage power supply, a pressurized housing containing a capacitor and switching elements, an intermediate trigger amplifier, and a crowbar switch assembly. A 75 nF Condenser Products EC753-80M capacitor is DC-charged by a Glassman -80 kV power supply [15]. A pressurized SF₆ gas switch provides a low inductance short to ground at the high voltage electrode of the capacitor [1]. The capacitor discharges a positive output pulse into a near open circuit formed by the first stages of Marx generator spark gaps [16]. The trigger resistors described earlier form trigger lines to each of the 30 spark gaps (Figure 2.13). Although it is not necessary to trigger each switch, this method may decrease overall breakdown time [17]. The crowbar assembly in Figure 2.14 is located in the low voltage end of the Marx tank. Spring-loaded pneumatic cylinders keep the capacitors and all high voltage supplies shorted to ground until the charge sequence is initiated.



Figure 2.12. Trigger generator



Figure 2.13. Gas and trigger lines



Figure 2.14. Crowbar assembly with input charging and triggering lines

2.5. Control Systems



Figure 2.15. Control cabinet

The master control system controls all major systems that are required for the operation of the Marx. These systems include charging, triggering, gas, and safety. Each of these systems will be discussed in detail.

The control system (Figure 2.16) monitors charging for all three power supplies. When the trigger generator's power supply reaches its preset charge voltage, the control system

indicates that the fire button can be pressed at any time, thus initiating the fire sequence. This feature can be expanded to include the Marx charging power supplies, but is currently disabled due to a non-compatible replacement supply. After the Marx has fired, the control system also disables the high voltage from the supplies. The replacement supply presently prevents this for the Marx supplies, but the trigger generator supply is still automatically disabled post-shot.

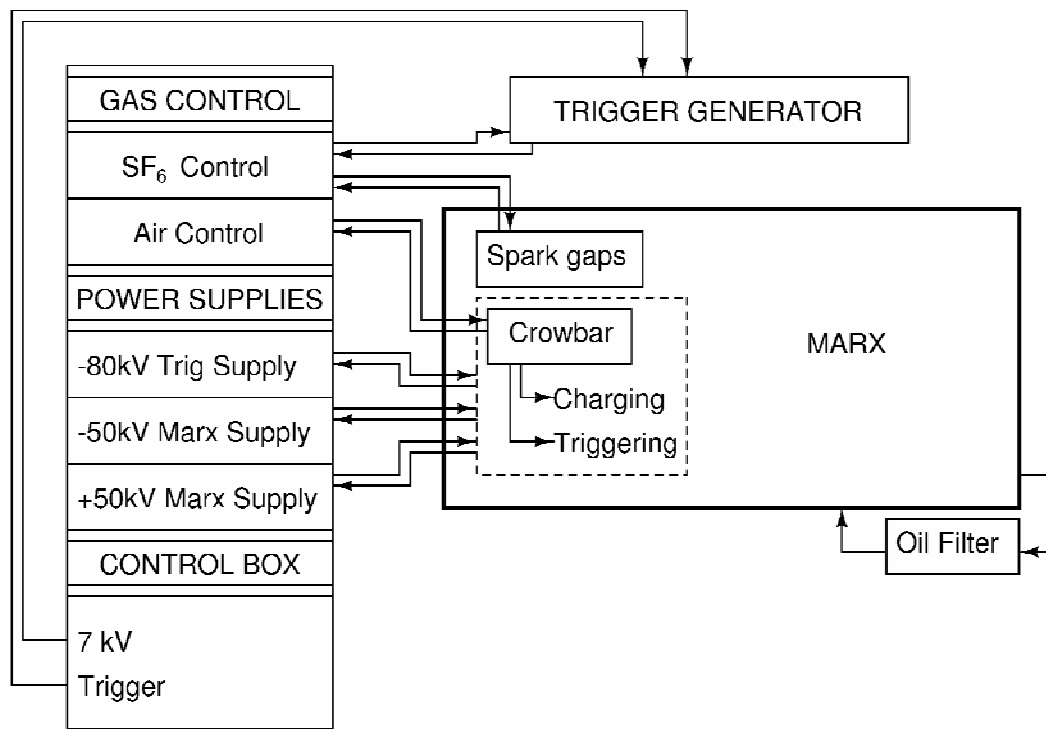


Figure 2.16. Control system block diagram

The triggering system is also monitored and operated by the control system. When the trigger generator is fully charged and the fire button is pressed, the control system sends a 7 kV trigger pulse to the trigger generator. The 7 kV pulse results in trigger switch breakdown and initiates the Marx spark gap trigger pulse.

The gas line pressures, both air and SF₆, are displayed above the control box. Venting of the lines is achieved with electronically-controlled valves. Regulators are also located on the gas control panel and allow for easy and controlled pressurization of the SF₆ for the Marx spark gaps and the trigger generator.

The safety system response consists of an automatic shutdown of the high voltage from the supplies and a crowbar of the supplies and capacitors to ground after a shot or during an abort of a shot. As discussed earlier, the automatic shut-off of the supplies only pertains to the trigger generator supply. The Marx supplies are still crowbarred to ground, but require a manual shutdown of high voltage. The crowbar (seen in Figure 2.14) shorts all high voltage supply cables and trigger lines to ground. It is physically located in the low voltage end of the tank and is pneumatically controlled by the control box.

2.6. Peaking Capacitor and Oil Switch

Positioned at the end of the thirty stages is a parallel plate oil dielectric peaking capacitor as shown in the photograph of Figure 2.17. The high voltage electrode of the self-break single-site oil switch is located in the center of the plate. The low voltage electrode is mounted inside a cylindrical oil-filled extension of the tank. The Marx is capable of operating with both large and small gap switch geometries. This fully-adjustable output switch allows for a variety of test parameters.



Figure 2.17. Peaking capacitor

The self-break single-site oil switch functions as the output switch of the Marx. The Marx generator requires an output switch for the capacitors to charge. If the capacitors were permanently connected to the load, the capacitors would never completely charge as it would dissipate into the load. The output switch of the UMC Marx is positioned at the end of the stage capacitors in the center of the peaking capacitor. Triggered by overvoltage, the switch arcs through the oil between the enhanced electrode (Figure 2.18) and the ball electrode.

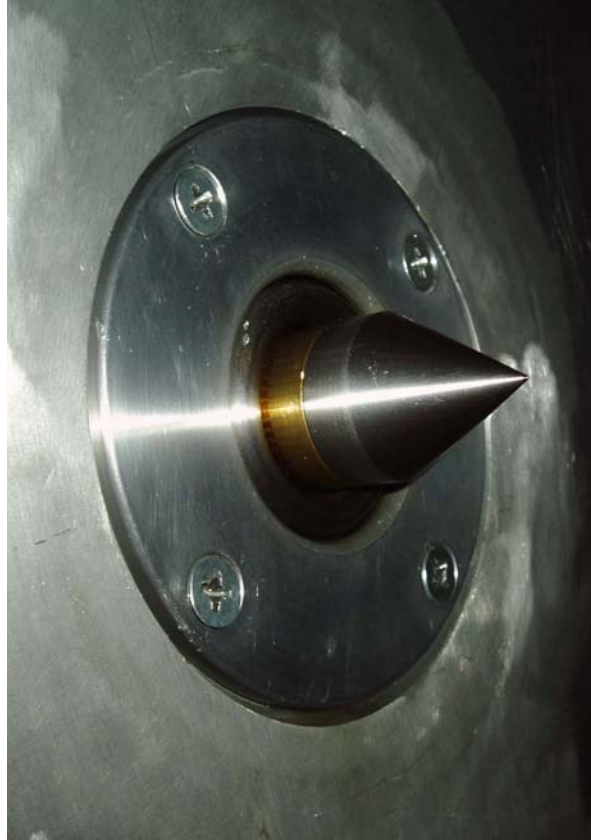


Figure 2.18. Oil switch enhanced electrode

The ball electrode is connected to four parallel load resistors with a total resistance of 300Ω . Using Grover's equation [18] for self-inductance of a circular single conductor under high frequency in Equation 2.2, the total inductance of the load (all four parallel resistors) is 35.6 nH. Also attached to the ball electrode is the post-switch voltage diagnostic described in Chapter 3.

$$L = 2 \cdot l \cdot \left(\ln \left(\frac{2 \cdot l}{r} \right) - 1 \right) \quad (2.2)$$

L = inductance (nH)

l = conductor length (cm), 24.3

r = conductor radius (cm), 0.9525

Peaking capacitors are often placed at the end of Marx generators with the desire of faster risetimes. The peaking capacitor in the UMC Marx has a value of 200 pF and is physically a parallel plate oil dielectric capacitor. With measurable dimensions and known dielectric properties of the insulator, the capacitance can be approximated by Equation 2.3.

$$C_{peak} = \frac{k\epsilon_0 A}{d} \quad (2.3)$$

$$\begin{aligned} C_{peak} &= \text{capacitance, } F \\ k &= \text{relative permittivity of oil, } 2.2 \\ \epsilon_0 &= \text{permittivity of space, } 8.854 \times 10^{-12} \text{ } F/m \\ A &= \text{area, } 1.03 \text{ } m^2 \\ d &= \text{separation, } 10 \times 10^{-2} \text{ } m \end{aligned}$$

Applying J. C. Martin's equation for breakdown [19], [20] to the peaker and the tank wall in Equation 2.4, it can be shown that for the 10 cm spacing, 5.4 MV would be required to achieve breakdown. With the Marx maximum operating voltage of 3 MV, the peaking capacitor is unlikely to prematurely breakdown before the output switch has fired. Since the value of k for transformer oil is independent of polarity, the above statement applies to both positive and negative Marx operation.

$$Ft^{1/3} A^{1/10} = k \quad (2.4)$$

$$\begin{aligned} F &= \text{breakdown field (} MV/cm \text{)} \\ t &= \text{time } (\mu s), 0.1 \\ A &= \text{electrode area (} cm^2 \text{), } 1030 \\ k &= 0.5 \text{ (for transformer oil)} \end{aligned}$$

In the simulation circuits described in detail in Chapter 4, the peaking capacitor is placed between the switch approximating the 30 spark gaps and the output oil switch. In the case of

the UMC Marx, the entire circuit can be simplified to the circuit shown in Figure 2.19. The low Marx inductance in combination with the peaking capacitor results in a theoretical UMC Marx output pulse 10-90% risetime of < 10 ns [1].

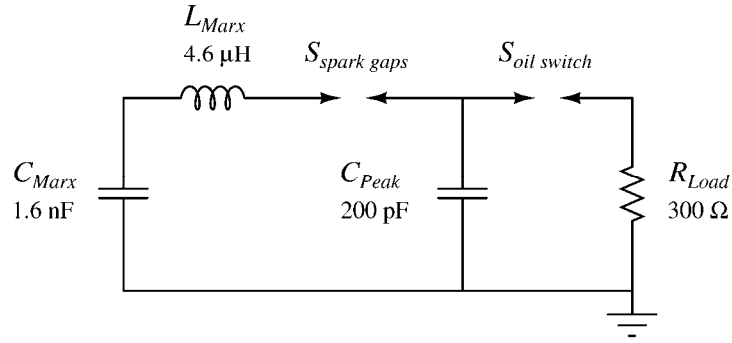


Figure 2.19. Simplified Marx with peaking capacitor

It can be determined that the peaking capacitor in the UMC Marx is not matched to the current load by using Equation 2.5 for an exponential decay though the load [21].

$$C_{peak} = \frac{\left(\frac{L_{Marx}}{R_{load}^2} \right)}{1 + \frac{L_{Marx}}{R_{load}^2 C_{Marx}}} \quad (2.5)$$

By that calculation, the peaking capacitor should be 50 pF. For the current peaking capacitor of 200 pF, a load resistance of 142 Ω would produce the ideal exponential decay. Minor adjustments of the CuSO₄ load resistor values for future experiments would optimize the circuit.

References for Chapter 2

- [1] “Spiral delay line pulser: operation and maintenance manual”, Pulse Sciences, Inc., PSI-O&M-2420, Dec. 1991.
- [2] “Diala AX data sheet,” Shell Lubricants, [Online]. Available: <http://www.shell-lubricants.com/products/pdf/DialaA&AX.pdf>
- [3] “Interline 850 data sheet”, International Protective Coatings, [Online]. Available: http://www.international-pc.com/pc/pds/850_us.pdf
- [4] “8300/04/10/14 Series Filter Assemblies”, Pall Corporation, [Online]. Available: <http://www.pall.com/variants/pdf/pdf/3112.pdf>
- [5] “Our capacitor specifications”, Condenser Products, [Online]. Available: <http://www.condenser.com/specs.htm>
- [6] Condenser Products, private communication, 2004.
- [7] “Instruction manual: WG series”, Glassman High Voltage Inc., PS/WG-50P6 M204250-01, July 1988.
- [8] “Series 1000 high voltage power supply owner’s manual”, Kaiser Systems, Inc., Varian IIS P/N E-81000065, 1991.
- [9] J. F. Francis, “High voltage pulse techniques”, Texas Tech University, 1976.
- [10] R. Beverly III and R. Campbell, “Aqueous-electrolyte resistors for pulsed power applications,” *Review of Scientific Instruments*, vol. 66, pp. 5625-5629, 1995.
- [11] R. Beverly III, “Application notes for aqueous-electrolyte resistors,” [Online]. Available: http://www.reb3.com/pdf/r_appl.pdf

- [12] “Tygon beverage tubing”, Saint-Gobain Performance Plastics Corporation, [Online].
Available:
<http://www.tygon.com/media/documents/S00000000000000001013/tygb443.pdf>
- [13] R. A. Fitch, “Marx – and Marx-like – high-voltage generators”, *IEEE Transactions on Nuclear Science*, vol. 18, no. 4, pp. 190-198, Aug. 1974.
- [14] “Series T-670 High Precision Spark Gap Switches”, Titan Corporation Pulse Sciences Division, [Online]. Available: <http://www.titanpsd.com/PDFs/T-670.pdf>
- [15] “Instruction manual: LG series”, Glassman High Voltage Inc., PS/LG-80N-1.5 M204210-01, July 1988.
- [16] “Pulser to study the effects of EMP induced signals on analog models of large antenna structures”, Pulse Sciences, Inc. PSI-P-87-355, Sept. 1987.
- [17] R. W. Morrison and A. M. Smith, “Overvoltage and breakdown patterns of fast Marx generators”, *IEEE Transactions on Nuclear Science*, vol. 19, no. 4, pp. 20-27, Aug. 1972.
- [18] F. W. Grover, *Inductance Calculations*, Dover, 1962.
- [19] J. C. Martin, “Nanosecond pulse techniques,” *Proceedings of the IEEE*, vol. 80, no. 6, pp. 934-945, Jun. 1992.
- [20] T. Martin, A. Guenther, and M. Kristiansen, Eds., *J. C. Martin on Pulsed Power*, New York: Plenum Press, 1996.
- [21] R. J. Adler, “Pulse power formulary,” North Star Research Corporation, [Online].
Available: <http://www.northstar-research.com/PDF/Formweb1.pdf>

CHAPTER 3. DIAGNOSTICS

3.1. Requirements

The UMC Marx oil switch test facility required two voltage diagnostics: before and after the output oil switch. It was necessary that these diagnostics minimally impact the system and accurately measure the performance of the pulser. Since typical, off-the-shelf voltage probes could not withstand the high peak voltages of the Marx output, other methods of determining voltage waveforms needed to be developed. It was desired that the voltage probes attenuate the Marx output pulse by a factor of 20,000 to safely acquire data with an oscilloscope. Liquid resistive voltage dividers were selected for the diagnostics.

The two measurements desired were voltages in the pre-switch and post-switch locations. The voltage waveform measured at the high voltage side of the output switch allows for monitoring of the capacitor charge. The charge level of the capacitors at the time the trigger pulse was applied can also be determined. The second voltage measurement required was on the output side of the switch in parallel with the load resistors. This measurement is possibly the more important of the two diagnostics since it monitors the operation of the oil switch and final output of the Marx.

The first probe developed was the post-switch divider due to its less accessible location at the end of the Marx in the oil-filled cylindrical extension of the tank. The output of the Marx arcs through the oil from the enhanced electrode to the ball electrode and then dissipates through the load resistors. The post-switch resistive voltage divider is positioned in parallel with

the load resistors. Minimizing the impact of the probe on the circuit, the resistance of the divider was included in the load resistance calculations.

The pre-switch divider needed to be placed inside the tank with the capacitors and attached to the top frame for ground. This divider had both extended space parameters and considerably easier access than the post-switch divider.

3.2. Voltage Divider Theory

Liquid resistive voltage dividers are simple, effective, and easy-to-build probes that are a cost-efficient solution to the need for a high voltage diagnostic. The circuit for the high voltage resistive probe is based on the simple voltage divider circuit in Figure 3.1 [1]. The input voltage V_1 is related to the output voltage V_2 by Equation 3.1. The ratio formed by the resistors R_1 and R_2 can be referred to as the division ratio [2]. Coaxial stray capacitance of the divider to the tank wall is calculated in Equations 3.2 and Equation 3.3. The resultant value of 10.7 pF distributed throughout the geometry can be assumed negligible for the UMC Marx configuration.

$$V_2 = V_1 \frac{R_2}{R_1 + R_2} \quad (3.1)$$

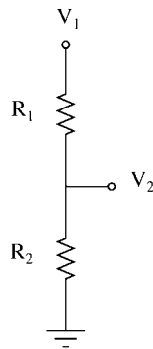


Figure 3.1. Voltage divider circuit

$$Z = \frac{60}{\sqrt{\epsilon}} \ln\left(\frac{D}{d}\right) \quad (3.2)$$

Z = impedance, 149 Ω

ϵ = dielectric constant, 2.2

D = outer conductor, inner diameter, 40 *in*

d = inner conductor, outer diameter, 1 *in*

$$C = \frac{\tau}{Z} \quad (3.3)$$

C = capacitance, 10.7 *pF*

τ = transit time in oil, 1.5 *ns/ft*

Z = impedance, 149 Ω

An expanded version of the voltage divider circuit is shown in Figure 3.2. The additional divider comprised of R_3 and R_4 is provided to match the line for reflection minimization.

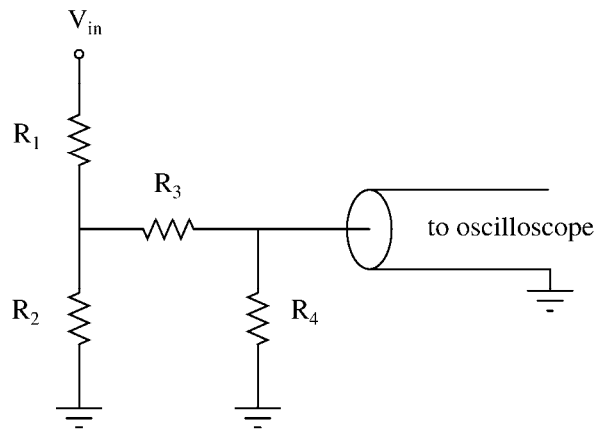


Figure 3.2. Simplified voltage divider implemented in diagnostic circuit

Physically, the probe consists of two stages [3]. The first stage is the liquid resistor portion which is responsible for the majority of the division ratio. It is built much like the liquid resistors discussed in Chapter 2 [4], [5] with 1 inch inner diameter Tygon B-44-3 beverage tubing

[6]. The resistor is shaped much like a typical resistor with two electrodes separated in an aqueous salt solution inside a sealed plastic tube. The difference from those previously described is the tap-off electrode. The tap-off electrode is positioned a small distance away from the electrode on the low voltage end of the resistor. It is isolated from the low voltage electrode through the middle by a section of RG-401 cable. Visually, the tap-off electrode can be noted in Figure 3.3 at a spacing of 1.5 mm from the low voltage electrode.

The major advantage of using a liquid resistor is that both parts of the resistor will maintain the same chemical composition regardless of the stresses applied. Knowing that the resistors are linear in an electric field between 2 – 50 kV/cm when $\rho = 60 - 1200 \Omega \text{ cm}$ enables the assumption that the division ratio will also remain constant [4], [5].



Figure 3.3. Voltage divider middle electrode

The second stage of the divider is composed of discrete resistors in a small, electrically shielded box. The RG-401 from the tap-off electrode is fed through one side of the box. A BNC connection for an RG-58 cable is located on the opposing side. This can be seen in Figure 3.4.

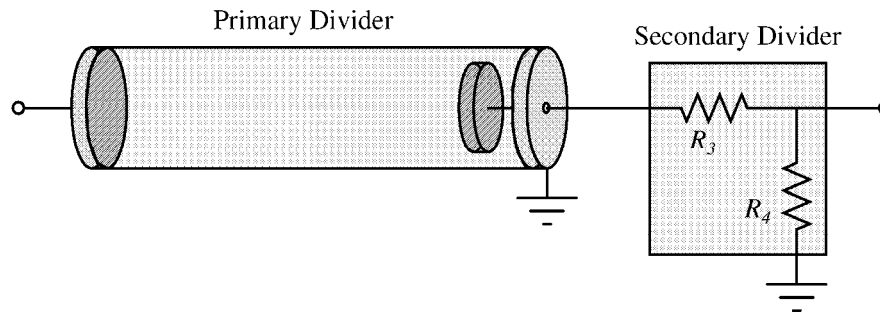


Figure 3.4. Voltage divider stages

From Figure 3.4, it can be noted that the primary divider is comprised of R_1 and R_2 . The tap-off electrode forms two resistors. The resistor R_1 is the larger of the two and consists of the region from the high voltage electrode to the tap-off electrode. Due to its large size, the resistor value can be approximated to be the entire resistance value from high to low voltage electrodes for measurement purposes. This resistor attenuates the input voltage down to a level compatible with the input to an oscilloscope. The second of the two copper sulfate resistors is physically located between the tap-off electrode and the low voltage electrode. This is a much smaller value with minimal voltage drop between the electrodes. The voltage on the middle electrode is transferred to the second stage of the voltage divider. The first of the secondary divider resistors, R_3 , can be used as a value to slightly adjust the output voltage. On the other hand, R_4 is used to match the output cable impedance so as to minimize reflections in the data. Consequently, R_4 is usually 50 Ω .

3.3. Post-switch Divider

The post-switch divider seen in Figure 3.5 had a limited space requirement of 10 inches. The resulting division ratio for the divider was 10,000:1. The CuSO_4 resistor contributed a

division of 200 and the discrete dividers added an additional division of 50. The post-switch divider is housed in the cylindrical oil-insulated extension at the end of the tank.

The total resistance of the liquid portion of the divider is $5\text{ k}\Omega$ as measured. In parallel with the load resistors, it has the effect of minimally lowering the load resistance from $300\ \Omega$ to $283\ \Omega$. With the inability to attain exact measurement values with CuSO_4 resistors, the load can be still approximated as $300\ \Omega$. One watt resistors were used for the discrete portion of the divider. The resistor R_3 has the value of $2.56\text{ k}\Omega$ and the resistor R_4 has the value of $48.43\ \Omega$.



Figure 3.5. Post-switch voltage divider

The inductance of the probe can be calculated with Grover's equation for self-inductance of a circular single conductor under high frequency [7]. Given the parameters described in Equation 3.4, the result is 101.3 nH .

$$L = 2 \cdot l \cdot \left(\ln \left(\frac{2 \cdot l}{r} \right) - 1 \right) \quad (3.4)$$

- L = inductance (nH)
 l = conductor length (cm), 25.4
 r = conductor radius (cm), 2.54

The capacitance of the probe can be calculated from both the high voltage electrode to the tap-off electrode and from the tap-off electrode to the low voltage electrode. Equation 3.5 and Equation 3.6 can be used to determine these values. The 404 femtofarads calculated between the high voltage electrode and the tap-off electrode are negligible. On the other hand, the capacitance of 239.2 pF between the tap-off electrode and the high voltage electrode should be factored into the frequency response of the probe.

$$C_{hv-tap} = \frac{k \epsilon_0 A}{d} \quad (3.5)$$

- C_{hv-tap} = capacitance, 404 fF
 k = relative permittivity of water, 80
 ϵ_0 = permittivity of space, $8.854 \times 10^{-12} F/m$
 A = area, $506.7 \times 10^{-6} m^2$
 d = separation, $889 \times 10^{-3} m$

$$C_{tap-lv} = \frac{k \epsilon_0 A}{d} \quad (3.6)$$

- C_{tap-lv} = capacitance, 239.2 pF
 k = relative permittivity of water, 80
 ϵ_0 = permittivity of space, $8.854 \times 10^{-12} F/m$
 A = area, $506.7 \times 10^{-6} m^2$
 d = separation, $1.5 \times 10^{-3} m$

Breakdown within the 10 inch (25.4 cm) probe is not a concern according to J. C. Martin's equation (Equation 3.7) [8], [9] which indicates that a positive voltage of 12 MV or a negative voltage of 24 MV would be required for breakdown.

$$Ft^{1/3} A^{1/10} = k \quad (3.7)$$

F = breakdown field (MV/cm)

t = time (μs), 0.1

A = electrode area (cm^2), 20.3

k_+ = 0.3 (for positive electrodes in water)

k_- = 0.6 (for negative electrodes in water)

3.4. Pre-switch Divider

The pre-switch divider seen in Figure 3.6 has a division ratio of 20,000:1. The $CuSO_4$ resistor portion accounts for a division of 400. Additional discrete resistors contribute a division of 50. The length of the pre-switch divider is approximately 35 inches.

The resistance of the liquid divider is also approximately 5 k Ω . The divider is attached to the shaper that forms the high voltage side of the peaking capacitor and to the top of the grounded frame. One watt resistors were used for the discrete portion of the divider. The resistor R_3 has the value of 2.46 k Ω and the resistor R_4 has the value of 48 Ω .

The inductance of the probe can be calculated with Grover's equation for self-inductance of a circular single conductor under high frequency [7]. Given the parameters described in Equation 3.8, the result is 577.6 nH.

$$L = 2 \cdot l \cdot \left(\ln \left(\frac{2 \cdot l}{r} \right) - 1 \right) \quad (3.8)$$

- L = inductance (nH)
- l = conductor length (cm), 88.9
- r = conductor radius (cm), 2.54

The capacitance of the pre-switch divider can be calculated from both the high voltage electrode to the tap-off electrode and from the tap-off electrode to the low voltage electrode using Equation 3.9 and Equation 3.10. The capacitance of 1.41 pF between the high voltage electrode and the tap-off electrode is slightly greater than the similar calculation for the post-switch divider. The value of C_{tap-lv} is the same as the previous calculation since the electrode spacing between the tap-off electrode and the low voltage electrode is identical in both cases. Breakdown within the 35 inch (88.9 cm) probe is not a concern according to J. C. Martin's equation (Equation 3.11) [8], [9] which indicates that a voltage of 43 MV would be required for breakdown.

$$C_{hv-tap} = \frac{k\epsilon_0 A}{d} \quad (3.9)$$

- C_{hv-tap} = capacitance, 1.41 pF
- k = relative permittivity of water, 80
- ϵ_0 = permittivity of space, $8.854 \times 10^{-12} F/m$
- A = area, $506.7 \times 10^{-6} m^2$
- d = separation, $254 \times 10^{-3} m$

$$C_{tap-lv} = \frac{k\epsilon_0 A}{d} \quad (3.10)$$

- C_{tap-lv} = capacitance, 239.2 pF
- k = relative permittivity of water, 80
- ϵ_0 = permittivity of space, $8.854 \times 10^{-12} F/m$
- A = area, $506.7 \times 10^{-6} m^2$
- d = separation, $1.5 \times 10^{-3} m$

$$Ft^{1/3} A^{1/10} = k \quad (3.11)$$

F = breakdown field (MV/cm)

t = time (μs), 0.1

A = electrode area (cm^2), 20.3

k_+ = 0.3 (for positive electrodes in water)

k_- = 0.6 (for negative electrodes in water)



Figure 3.6. Pre-switch voltage divider

3.5. Calibration

Calibration of the resistive voltage dividers was done using a high voltage self-break and triggered-break switch with a Tektronix P6015A high voltage probe [10]. Both the analog Tektronix 2467B and digital Tektronix TDS3034 [11] oscilloscopes were used to calibrate the

dividers. The +50 kV Glassman high voltage power supply [12] from the charging circuits discussed earlier was utilized for the tests. The configuration used for this calibration is seen in Figure 3.7. Although, the ideal calibration scenario is to test within the actual circuit parameters, this was not possible for the UMC Marx due to physical constraints. Data from the calibration of both the post-switch and pre-switch dividers can be seen in the plots following.

It can be noted from the calibration plots for the post-switch voltage divider (Figure 3.8 and Figure 3.9) that the risetimes and fall times are identical. This accuracy allows for exceptional data collection from the output of the Marx. The pre-switch divider was originally constructed without using a RG-401 cable connection to the tap-off electrode. Instead, a conductor and insulator without a matching 50Ω impedance was used. The result is a series of reflections in the output pulse. This can be seen in the pre-switch calibration data in Figure 3.10.

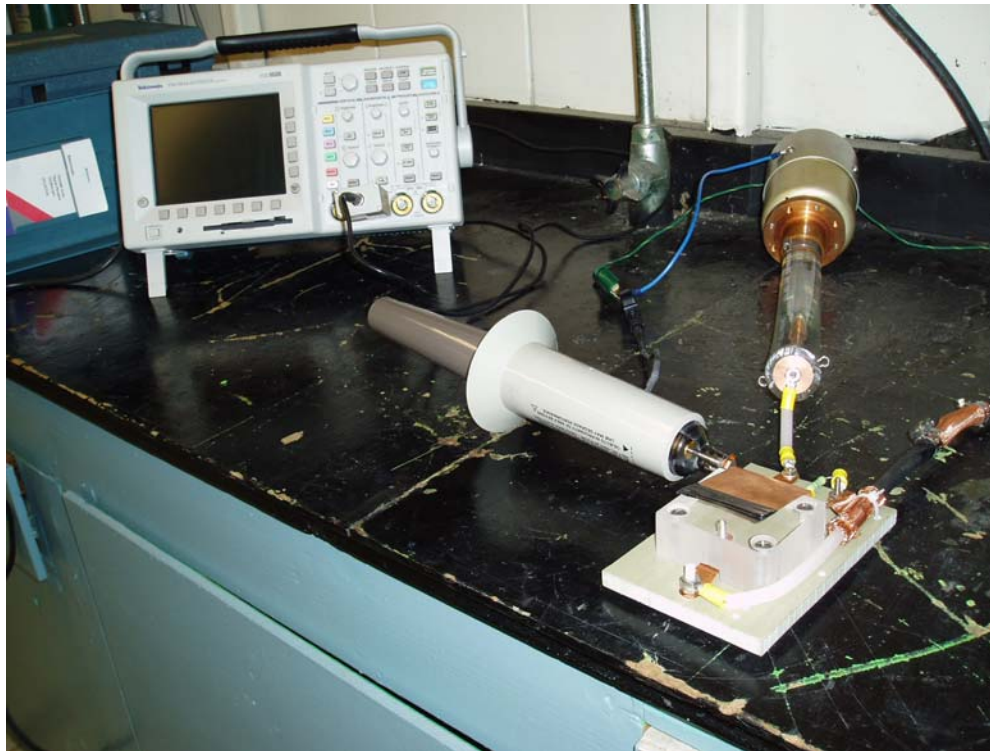


Figure 3.7. Voltage divider calibration configuration

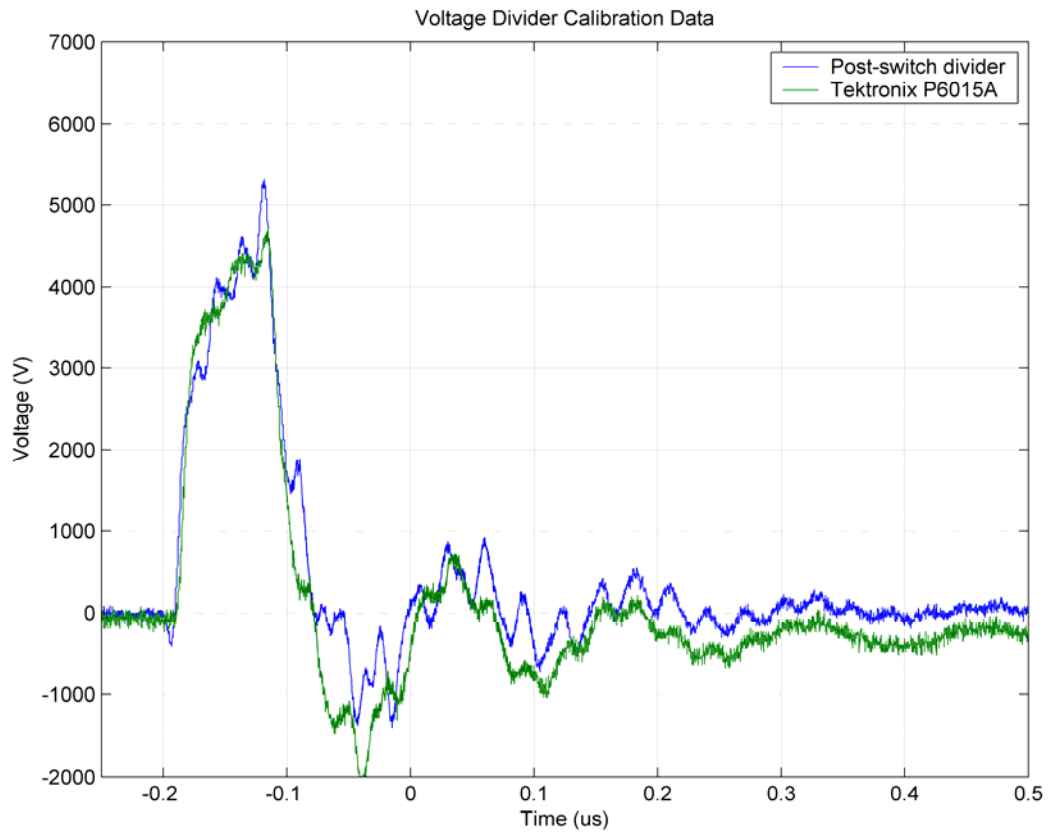


Figure 3.8. Digital calibration of post-switch divider

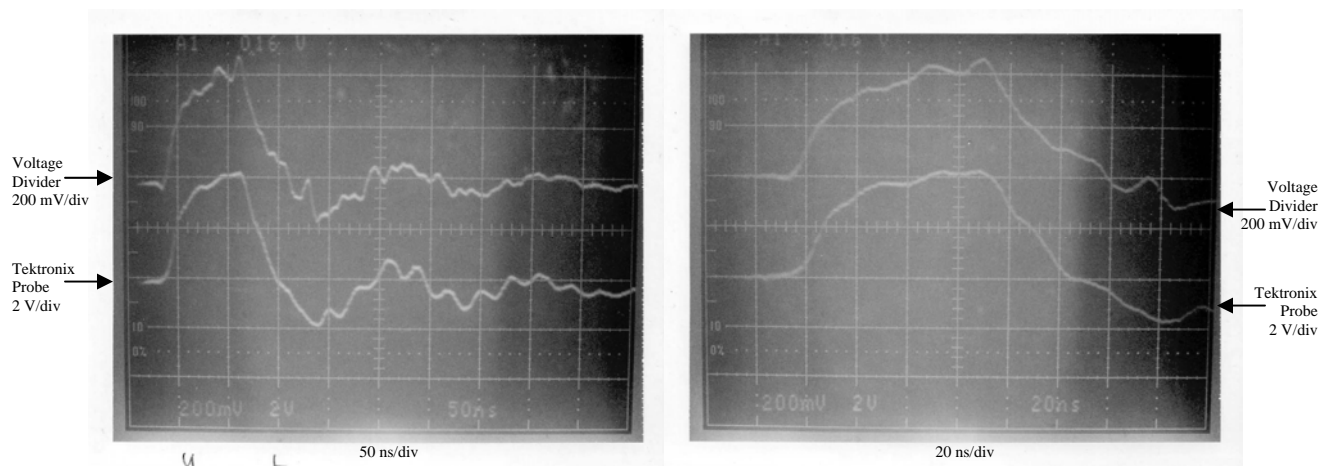


Figure 3.9. Analog calibration of post-switch divider

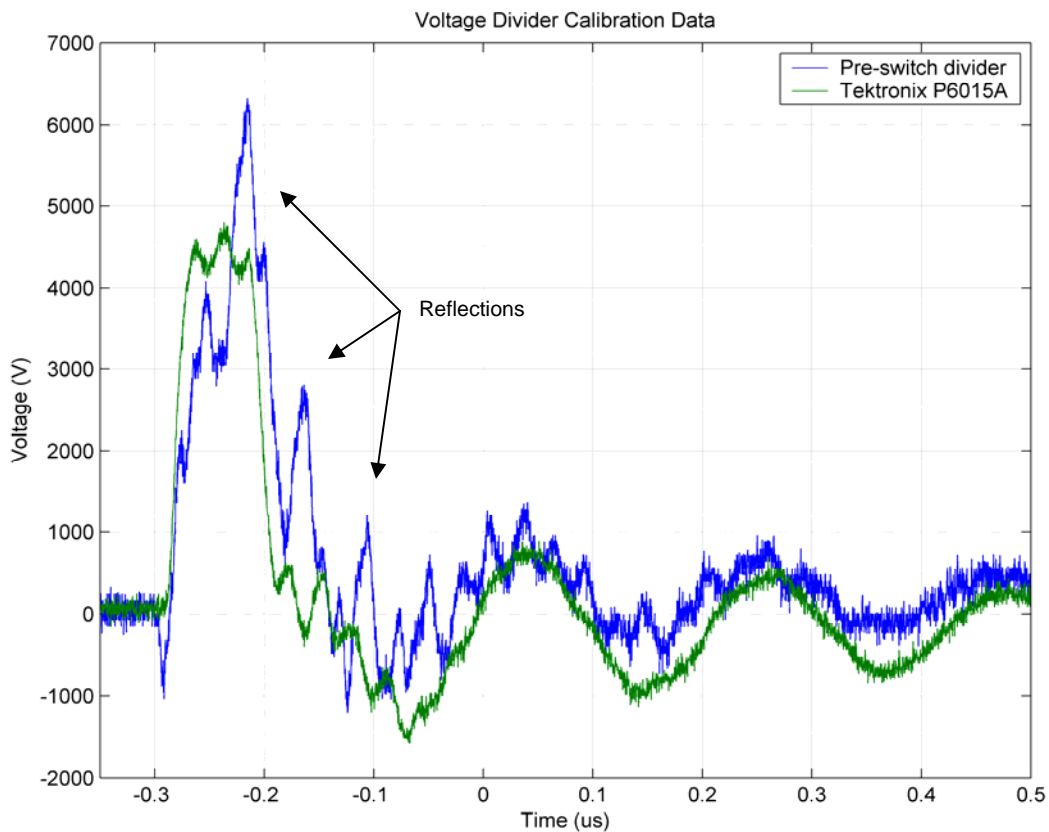


Figure 3.10. Digital calibration of pre-switch divider

During operation of the Marx, the voltage dividers are located in their respective locations and the oscilloscope is located in a copper-mesh Faraday cage seen on the right-hand side of Figure 3.11. The copper sheet in the figure lies underneath the cables as a path to the shielded cage. Despite the many opportunities for signal interference in a pulsed power system [13], the output pulses recorded and discussed in Chapter 5 provide great clarity for all necessary tests.



Figure 3.11. Diagnostic output connections and Faraday cage

References for Chapter 3

- [1] J. F. Francis, "High voltage pulse techniques", Texas Tech University, 1976.
- [2] A. J. Schwab, *High-Voltage Measurement Techniques*, MIT Press, 1972.
- [3] D. G. Pellinen and I. Smith, "A reliable multimegavolt voltage divider", *Review of Scientific Instruments*, vol. 43, pp. 299-301, 1972.
- [4] R. Beverly III and R. Campbell, "Aqueous-electrolyte resistors for pulsed power applications," *Review of Scientific Instruments*, vol. 66, pp. 5625-5629, 1995.
- [5] R. Beverly III, "Application notes for aqueous-electrolyte resistors," [Online]. Available: http://www.reb3.com/pdf/r_appl.pdf
- [6] "Tygon beverage tubing", Saint-Gobain Performance Plastics Corporation, [Online]. Available: <http://www.tygon.com/media/documents/S00000000000000001013/tygb443.pdf>
- [7] F. W. Grover, *Inductance Calculations*, Dover, 1962.
- [8] J. C. Martin, "Nanosecond pulse techniques," *Proceedings of the IEEE*, vol. 80, no. 6, pp. 934-945, Jun. 1992.
- [9] T. Martin, A. Guenther, and M. Kristiansen, Eds., *J. C. Martin on Pulsed Power*, New York: Plenum Press, 1996.
- [10] "Passive High Voltage Probes", Tektronix, [Online]. Available: http://www.tek.com/site/ps/56-10262/pdfs/56W_10262.pdf
- [11] "Digital phosphor oscilloscopes data sheet" Tektronix, [Online]. Available: http://www.tek.com/site/ps/3G-12482/pdfs/3GW_12482.pdf

[12] “Instruction manual: WG series”, Glassman High Voltage Inc., PS/WG-50P6
M204250-01, July 1988.

[13] E. Thornton, *Electrical Interference and Protection*, Ellis Horwood, 1991.

CHAPTER 4. MODELING OF MARX

4.1. Marx Circuits

The basic Marx circuits described in Chapter 1 were enhanced to show the detailed parameters of the UMC Marx in Chapter 2. For modeling and simulation purposes, the expanded Marx circuit drawing in Figure 2.2 was simplified to the circuit shown in Figure 4.1. This equivalent circuit is appropriate for simulations of the erected Marx since the firing of all stages occurs nearly simultaneously and appears to the load as a single capacitive energy store [1]. The Marx capacitance C_{Marx} is the equivalent total capacitance of all the stages of the Marx. The Marx inductance L_{Marx} is the total series inductance of the Marx and all its connections.

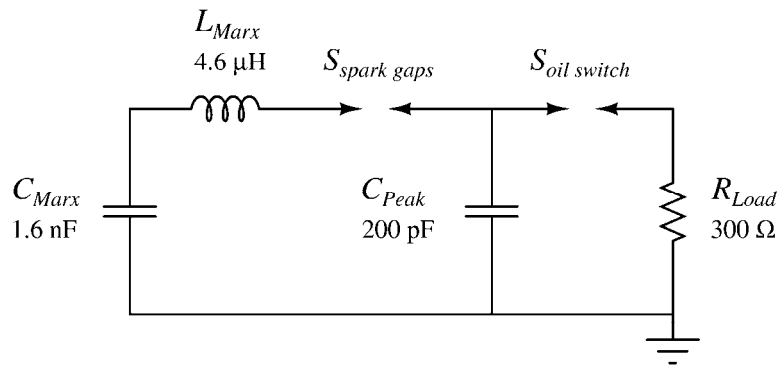


Figure 4.1. Simplified 30 stage UMC Marx circuit

4.2. PSPICE Simulations

Simulations were run on the Marx parameters for several different reasons. Determining the expected output of the Marx is important for both operational and safety concerns. By

determining the output pulse specification details before a shot is taken, the diagnostics can be optimized to accurately verify pulse shape. The PSPICE [2] simulations of the Marx both with and without the peaking circuit are shown in Figure 4.2. The PSPICE code for these results is documented in Appendix B. The ripple in the pulse from the simulation of the Marx with the peaking circuit is a result of the peaking capacitor and load producing a non-ideal exponential decay as described earlier in Chapter 2. The characteristics of the two pulses are outlined in Table 4.1 and Table 4.2. The risetime of 30 ns from the simulation without the peaking circuit can be attributed to the low inductance of the Marx and the triggering of all spark gaps simultaneously. The introduction of the peaking circuit to the Marx improves the risetime by an additional 20 ns.

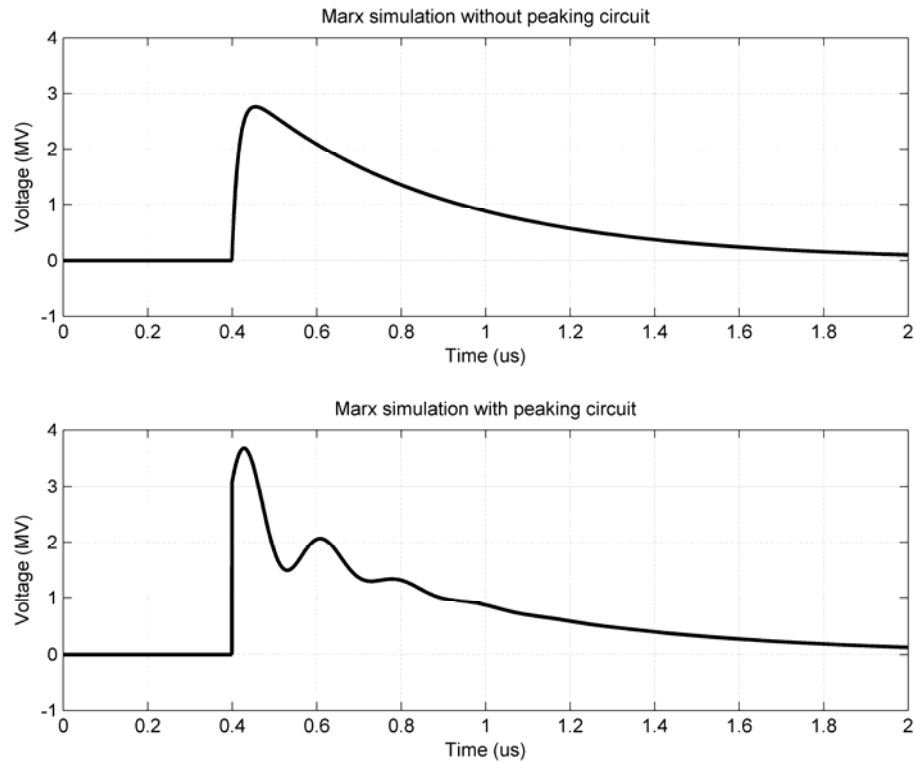


Figure 4.2. Simulated Marx output pulse with and without peaker

Table 4.1. Pulse characteristics from Marx simulation without peaking circuit

Risetime (10-90%)	30 ns
Pulse width (90-90%)	90 ns
Fall time (10-90%)	1.6 μ s

Table 4.2. Pulse characteristics from Marx simulation with peaking circuit

Risetime (10-90%)	10 ns
Pulse width (90-90%)	50 ns
Fall time (10-90%)	1.6 μ s

4.3. Breakdown Calculations

To verify the functionality of the Marx at specific output switch spacings, voltage breakdown calculations were computed. The Bouwers and Cath [3], [4] electric field strength configurations (described in Figure 4.3 and Figure 4.4) with variable separation produced the results given in Figure 4.5. For sphere-sphere calculations, the electrodes were approximated as two spheres with diameters of 3 cm. For sphere-plane calculations, the enhanced electrode was approximated as a sphere with the same diameter (0.28 cm) as the tip of the electrode. Since these are both approximations, the actual result lies between the two.

For comparison, the J. C. Martin [5], [6] liquid breakdown equation (Equation 4.3) was used to compute the oil breakdown of a 300 ns pulse with the electrode geometry used in the sphere-sphere calculation. The result in Figure 4.5 indicates that the output switch can be successfully operated at all voltages (500 kV – 3 MV) required for future high pressure switch tests. Given that the actual maximum electric field of the output switch is between the two calculations described earlier, the breakdown fields from the J. C. Martin equation occur on the low side of the two. It appears that the only area in which breakdown has a slightly greater

chance of not occurring is at voltages under 1 MV and gap spacings under 4 cm. Decreasing the gap further with electrode geometry changes would rectify this issue. During fabrication of future electrodes, the length could be easily extended if operation at lower voltages is required. Overall, the comparison of the maximum electric fields to the Martin equation suggests that the Marx will work appropriately within the given parameters.

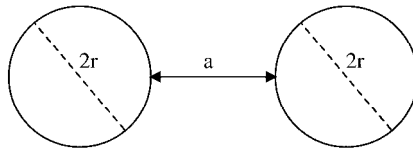


Figure 4.3. Two spheres with equal radii

$$E_{\max} = 0.9 \cdot \frac{V}{a} \cdot \frac{r + a/2}{r} \quad (4.1)$$

- E_{\max} = maximum electric field, MV/cm
- V = potential difference between electrodes, MV
- a = electrode spacing, 3-7 cm
- r = electrode radius (approx. sphere), 1.5 cm

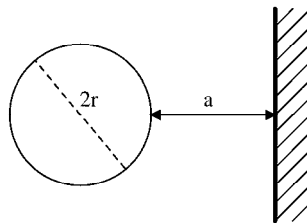


Figure 4.4. Sphere and plane

$$E_{\max} = 0.9 \cdot \frac{V}{a} \cdot \frac{r + a}{r} \quad (4.2)$$

- E_{\max} = maximum electric field, MV/cm
- V = potential difference between electrodes, MV
- a = electrode spacing, 3-7 cm
- r = electrode radius (approx. point), 0.14 cm

$$Ft^{1/3} A^{1/10} = k \quad (4.3)$$

F = breakdown field (MV/cm)

t = time (μs), 0.3

A = electrode area (cm^2), 7.07

k = 0.5 (for transformer oil)

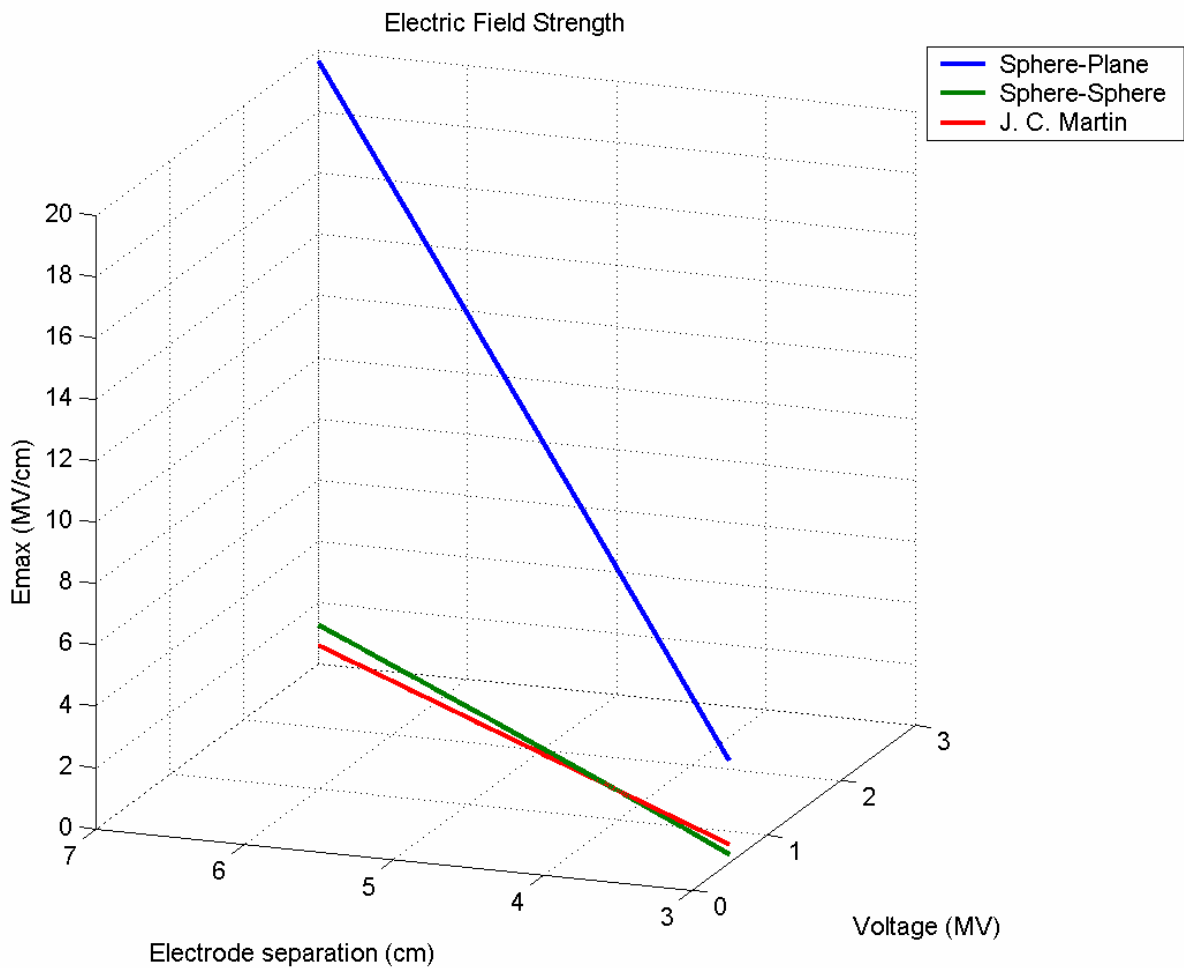


Figure 4.5. Electric field calculations with variable voltage and electrode separation

Additionally, the field enhancement factor (FEF) for the two electrode approximations can be calculated using Equation 4.4.

$$FEF = \frac{E_{max}}{E_{mean}} \quad \text{where} \quad E_{mean} = \frac{V}{a} \quad (4.4)$$

- V = potential difference between electrodes, MV
- a = electrode spacing, 3-7 cm

The result from this equation with both electrode approximations is shown in Figure 4.6.

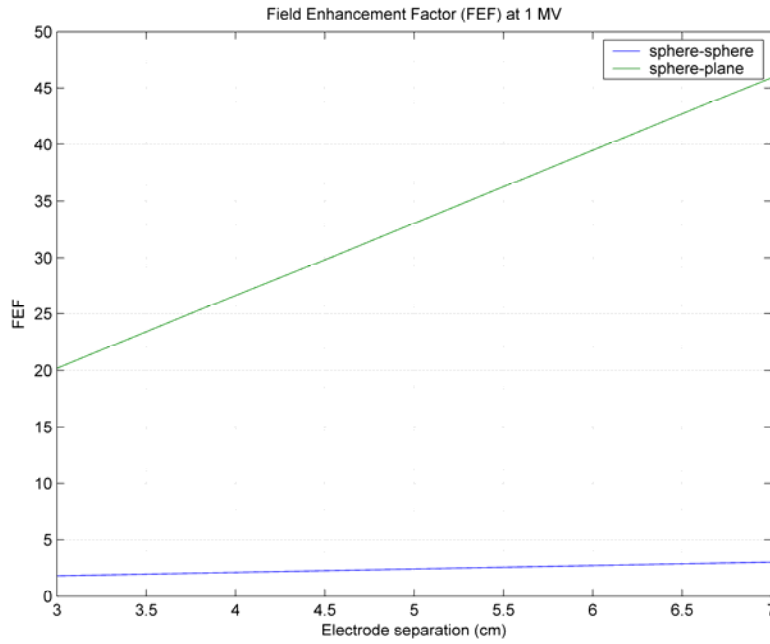


Figure 4.6. Field enhancement factor for sphere-sphere and sphere-plane geometries

The FEF for the sphere-plane geometry is significantly higher than the FEF for the sphere-sphere geometry. The electric field strengths with the same electrode separation distances are seen in Figure 4.7. Since the electrodes resemble the sphere-sphere approximation with slight enhancement, it appears likely that an electric field of at least 0.5 MV/cm will occur with a 5 cm

separation. The red line representing the mean voltage across the gap can be interpreted as the minimum due to the field enhancement design present in the pointed high-voltage electrode. This can be further verified with the electrostatic simulations in the next section.

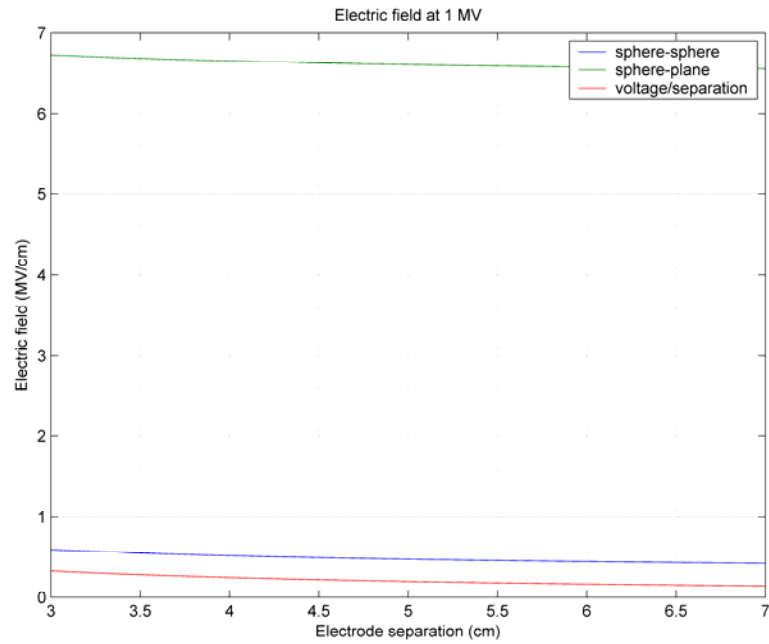


Figure 4.7. Electric field strength with varying electrode separation

4.4. Electrostatic Simulations

Electrostatic simulations were conducted on the geometry of the output switch to verify proper breakdown. The cross-sectional simulation results seen in the following Quickfield [7] color maps were a product of a 1 MV charge with a 5 cm gap spacing. Figure 4.8 is a mapping of the field strengths before the Marx has fired. Vectors of field strengths were also included on the plots.

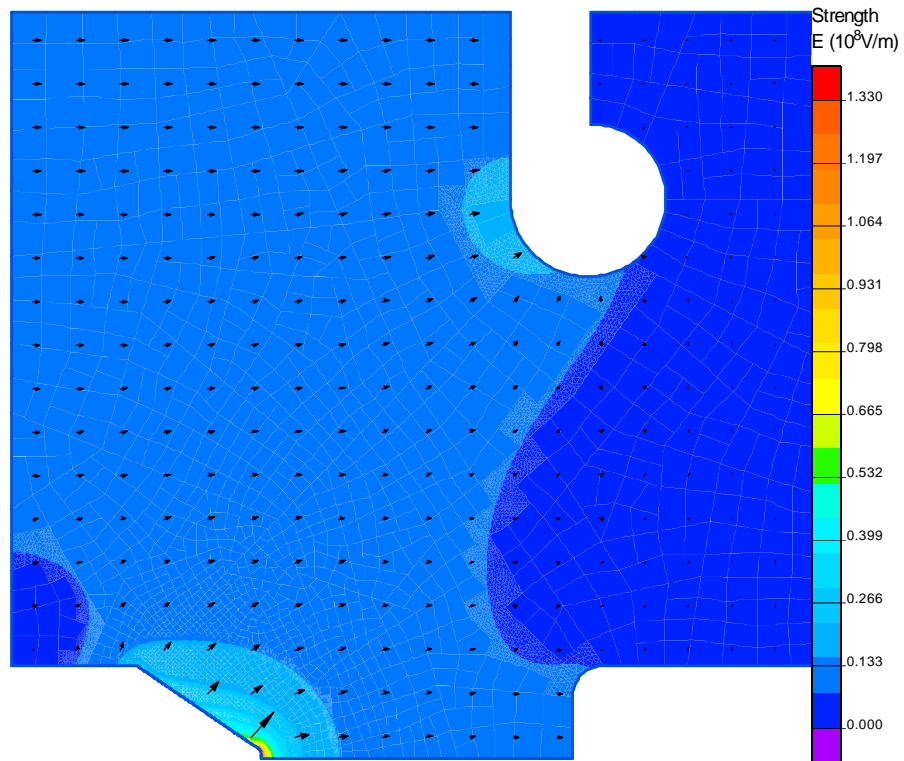


Figure 4.8. Electrostatic simulation of output switch field strength before Marx fires

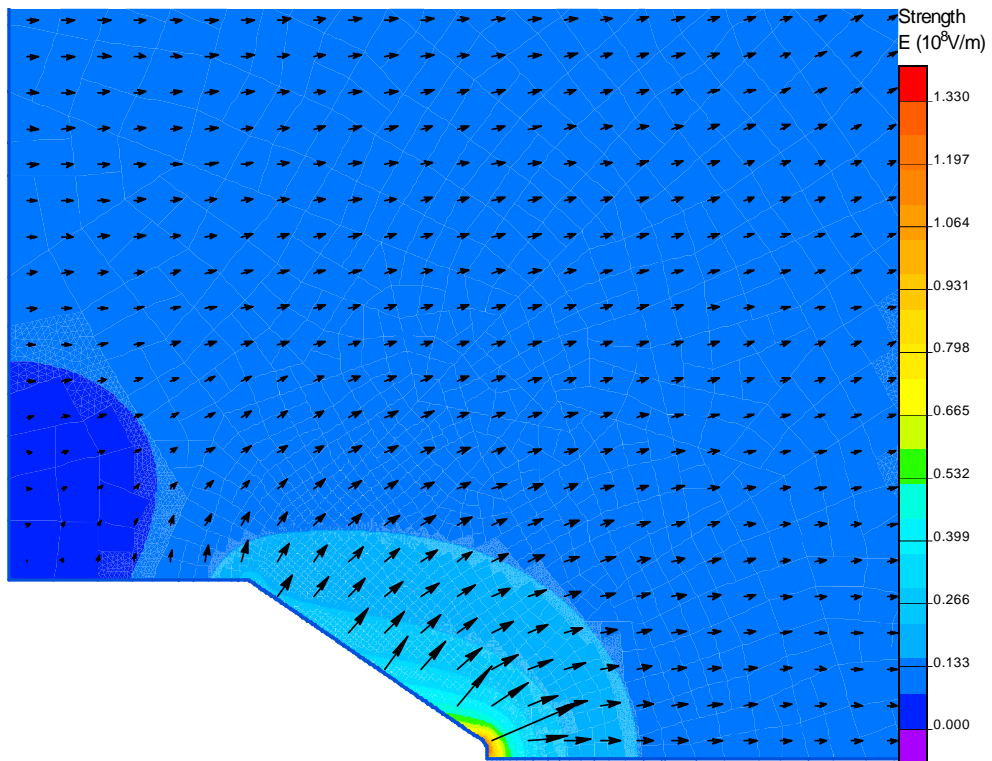


Figure 4.9. Enlarged view of tip of enhanced electrode electric field strengths

The field strength values from the Quickfield simulations coincide with the electric field calculations in the previous section. From the enlarged view of the enhanced electrode in Figure 4.9, the maximum electric field strength attains a value of 1.33 MV/cm. This result is greater than the 0.48 MV/cm sphere-sphere geometry approximation. As mentioned earlier, this was expected due to the enhanced tip on the high-voltage electrode. The 1.33 MV/cm field strength from Quickfield results in a FEF of 6.65 with a 5 cm electrode separation. Comparing this result to the plot in Figure 4.6, the UMC Marx configuration is more closely approximated by the sphere-sphere geometry approximation than the sphere-plane geometry approximation.

It is interesting to note that the electric fields on the field shaper ring in the Quickfield simulations appear to have a noticeable effect on the output switch. The experimental result from this is discussed in Chapter 5. The possibility of moving the low voltage electrode from its current, recessed position is an option for future experiments. The gradient of potentials surrounding the switch is seen in Figure 4.10 with expected results.

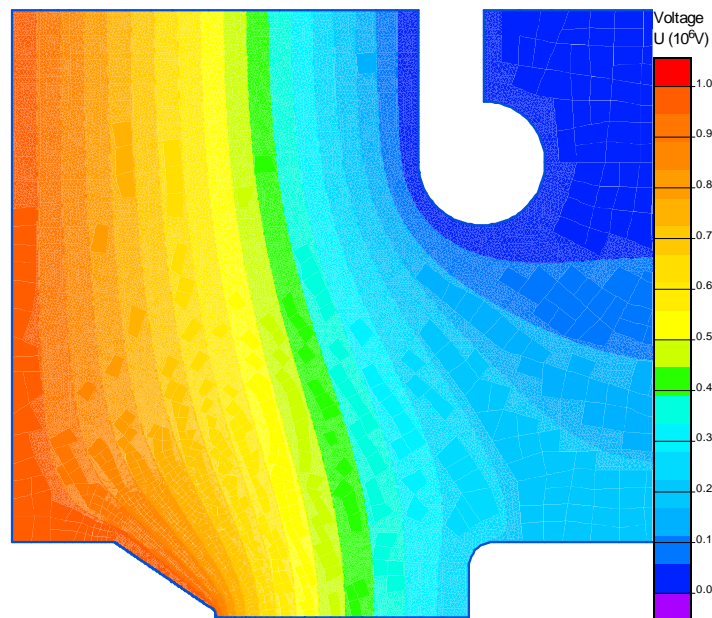


Figure 4.10. Electrostatic simulation of output switch potentials before Marx fires

References for Chapter 4

- [1] J. F. Francis, "High voltage pulse techniques", Texas Tech University, 1976.
- [2] Orcad 9.1 [Online]. Available: www.orcad.com
- [3] A. Bouwers and P. G. Cath, "The maximum electric field strength for several simple electrode configurations," *Philips Tech. Review*, vol. 6, no. 9, pp. 270-278, 1941.
- [4] W. D. Greason, *Electrostatic Discharge in Electronics*, Research Studies Press Ltd., 1992.
- [5] J. C. Martin, "Nanosecond pulse techniques," *Proceedings of the IEEE*, vol. 80, no. 6, pp. 934-945, Jun. 1992.
- [6] T. Martin, A. Guenther, and M. Kristiansen, Eds., *J. C. Martin on Pulsed Power*, New York: Plenum Press, 1996.
- [7] Quickfield [Online]. Available: www.quickfield.com

CHAPTER 5. SWITCH EXPERIMENTS

5.1. Experimental Setup

After the results from the previous chapter, it was determined that a 1 MV output pulse from the Marx would be an appropriate test for its functionality without overstressing its components. The 1 MV output from the Marx will be described specifically in this section. Parameters to be discussed include charging voltages, triggering voltages, gas pressures, and switch gap spacings. Testing was conducted by varying these parameters to check both system versatility and simulation verification.

For a 1 MV output with 30 stages, each stage was charged to 33.3 kV. Since the charging schematic utilizes dual-polarity charging, half of each stage was charged to +16.7 kV and half was charged to -16.7 kV. Applying these charge voltages to Figure 5.1 [1], it was appropriate to pressurize the spark gaps with SF₆ to 4 psi. Using the original operation manual guidelines to charge the trigger generator to approximately twice the half-stage voltage, the trigger generator was typically charged to 40 kV. Figure 5.2 [1] indicated the trigger generator should be pressurized to 22 psi. These values combined with a gap spacing number of 180 from Figure 5.3 [1] proved reliable for the Marx to fire 1 MV shots consistently. All three of the following original operation manual plots were verified by observing the parameter guidelines with the testing of the Marx. The test points from the current Marx operation fall along the same plot lines with the exception of the oil switch operating curve where changes in operation have been noted.

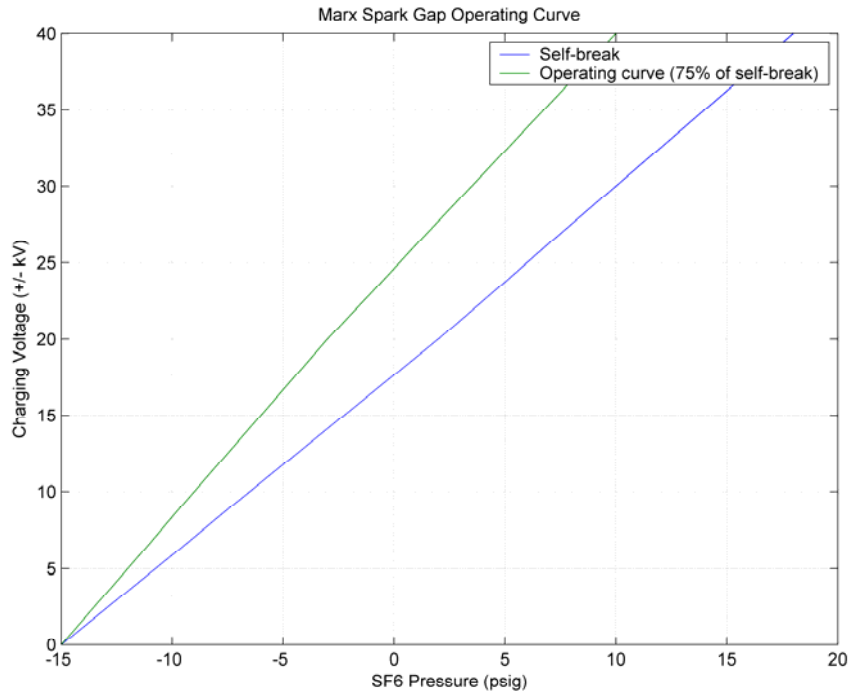


Figure 5.1. Marx spark gap operating curve [1]

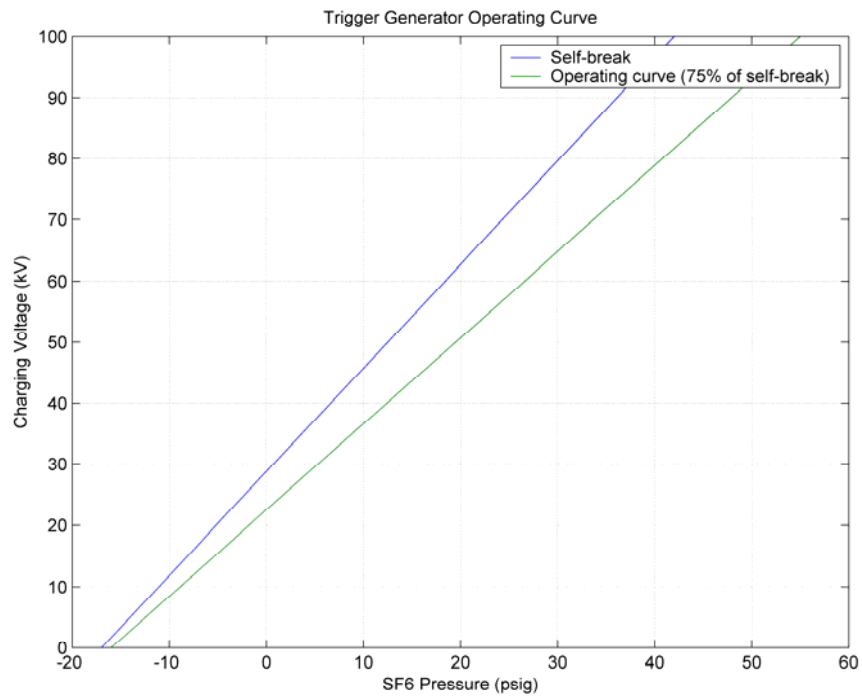


Figure 5.2. Trigger generator operating curve [1]

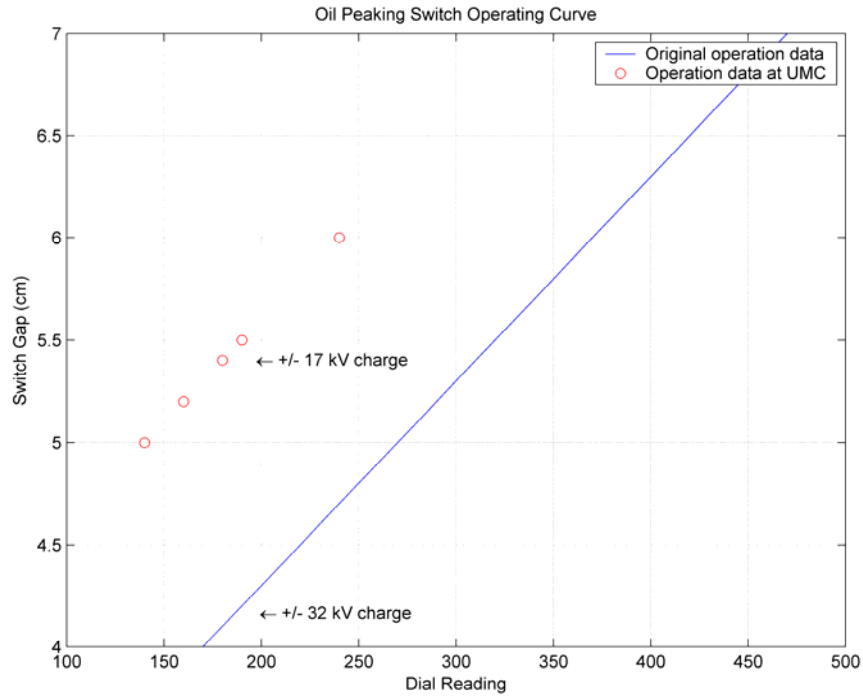


Figure 5.3. Oil peaking switch operating curve [1]

The quality of the shots was greatly dependent on oil filtration. As mentioned in Chapter 2, the output switch of the Marx is an oil dielectric switch. The quality of the Diala AX [2] used to insulate the Marx directly affected the arc formation across the output switch. It was visually noted that multiple arc channels formed after sets of shots without filtering between them. Large multi-channel arcs produced very large carbon clouds and bubbles that appeared to release smoke (or carbon) when they reached the surface. These multi-channel arcs began at the enhanced, high-voltage electrode and reached both the low-voltage electrode and the grounded field shaper (seen in the electrostatic simulations in the previous chapter). From the simulations conducted before the Marx was fired, it was known that the field shaper had higher electric field strengths than the recessed low-voltage electrode. As mentioned earlier, the possibility of moving the low voltage electrode closer to the high-voltage electrode is an option for future testing. Oil impurities appeared to increase the probability of the multi-channels occurring.

Pumping the oil through the filter located in the side of the tank for 20-30 minutes between shots proved sufficient to eliminate breakdown. Preparation for Marx operation and detailed records of individual shots are given in Appendix C and D respectively.

5.2. Experimental Results

Initial testing of the Marx was conducted using the point-ball electrode geometries discussed in the previous chapter. The tests have shown expected and repeatable results. Output pulse characteristics are listed in Table 5.1. The risetime of 18 ns represents a slight increase from the simulated results which could be attributed to bandwidth filtering within the oscilloscope. Waveforms from the post-switch divider at an output voltage of 1 MV are shown in Figure 5.4. The repeatability of the pulser can be noted from these waveforms. Comparing the experimental waveforms to the simulated waveform in Figure 5.5, the results are similar. The ringing in the experimental data appears to have a slightly larger influence on the pulse than in simulated results. Figure 5.6 shows output from both the pre-switch and post-switch dividers on the same plot. As indicated in Chapter 3, the pre-switch divider contains reflections due to impedance differences between the tap-off electrode and the 50 Ω cable.

Table 5.1. Output pulse characteristics

Risetime (10-90%)	18 ns
Pulse width (90-90%)	50 ns
Fall time (10-90%)	1.6 μ s

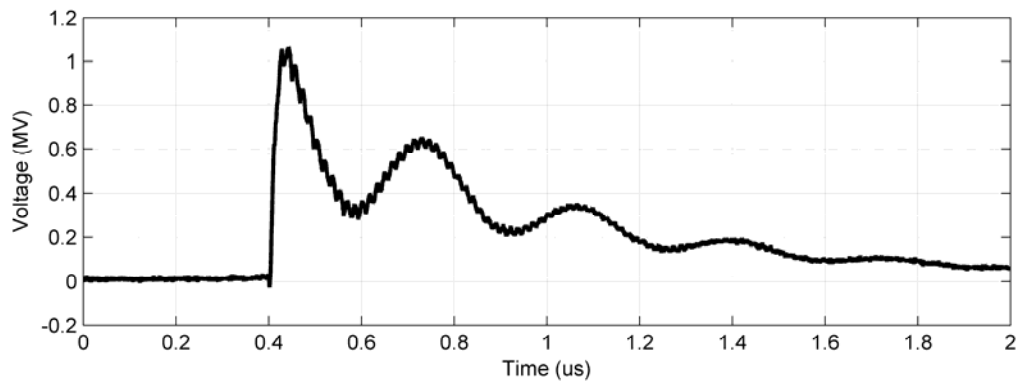
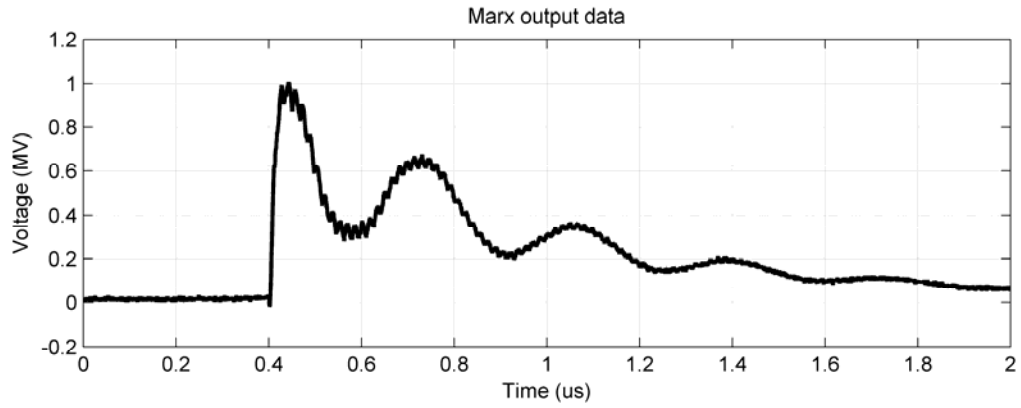


Figure 5.4. Marx output data

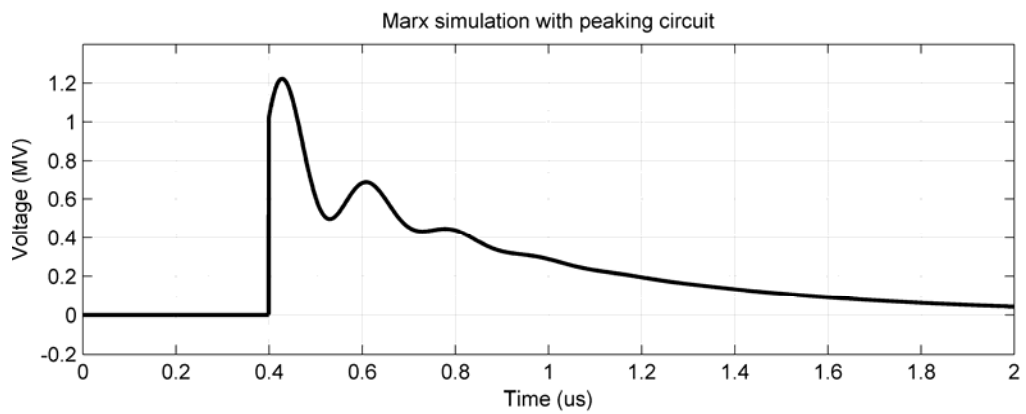


Figure 5.5. Marx simulated output

From the early results, the necessity for proper oil filtration was apparent. As discussed, the presence of certain levels of both carbon particles and bubbles occasionally facilitated arcs to

ground during the switching of the pulse. When multiple plasma channels contacted the grounded field shaper during a shot, at least one of the channels always made contact with the low-voltage electrode. An example of data from a shot when multi-channeling occurred can be seen in Figure 5.7. This data can be compared to the J. C. Martin equation [3],[4]. It can be observed from the plot that the arc initially contacted the low voltage electrode and later broke off to ground resulting in an approximate pulse width of 0.5 μ s. With an electrode area A of 7.07 cm² (radius 1.5 cm) and k equaling 0.5 for transformer oil, the result of the Martin equation is seen in Equation 5.1.

$$F = \frac{k}{t^{1/3} A^{1/10}} = 518 \text{ kV/cm} \quad (5.1)$$

This result indicates a likelihood of breakdown at 518 kV/cm across the gap. In actuality, with a charge voltage of 1.2 MV and a gap spacing of 5.4 cm, there was a mean electric field of 222 kV/cm across the gap. With the FEF of 6.65 determined in the previous chapter, the maximum electric fields were closer to 1.48 MV/cm. This exceeds the field strength necessary for breakdown according to the Martin equation. The impurities present in the unfiltered oil near the switch area assist in the formation of the extra channels. Additionally, a small misalignment was noted after the shot indicating the high-voltage electrode was closer to ground than originally calibrated.

Because the insulating oil quality was so important to the breakdown of the output switch, additional breakdown tests were conducted with a Hipotronics OC60D [5] ASTM D877 dielectric tester on a sample of the Diala AX from the switch area of the tank. Results are shown in Figure 5.8 and appear to slightly diverge from the manufacturer's specifications of breakdown voltages greater than 35 kV RMS [2].

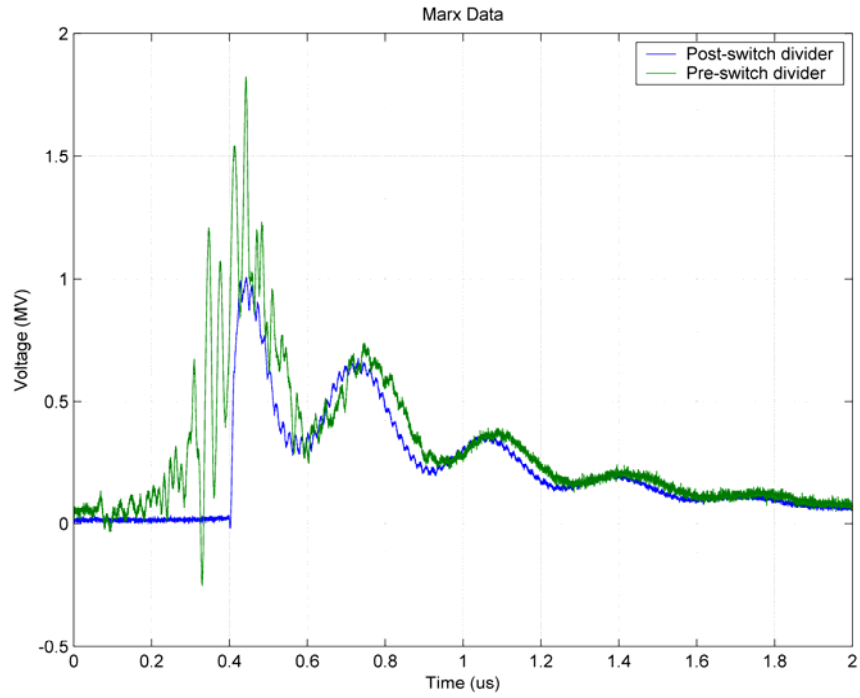


Figure 5.6. Data from both pre and post-switch dividers (Shot 8)

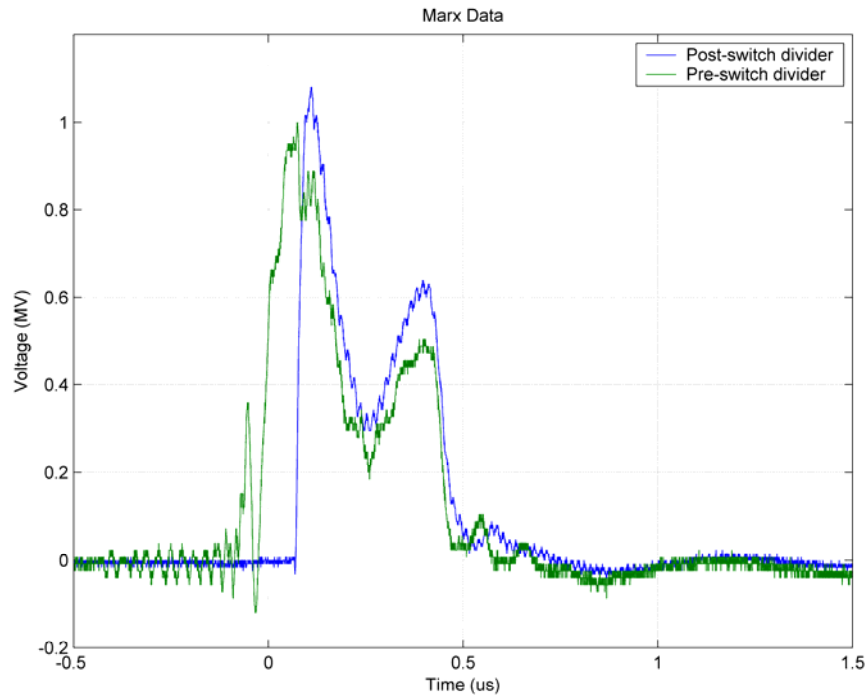


Figure 5.7. Marx shot with multi-channel arcs to ground (Shot 33)

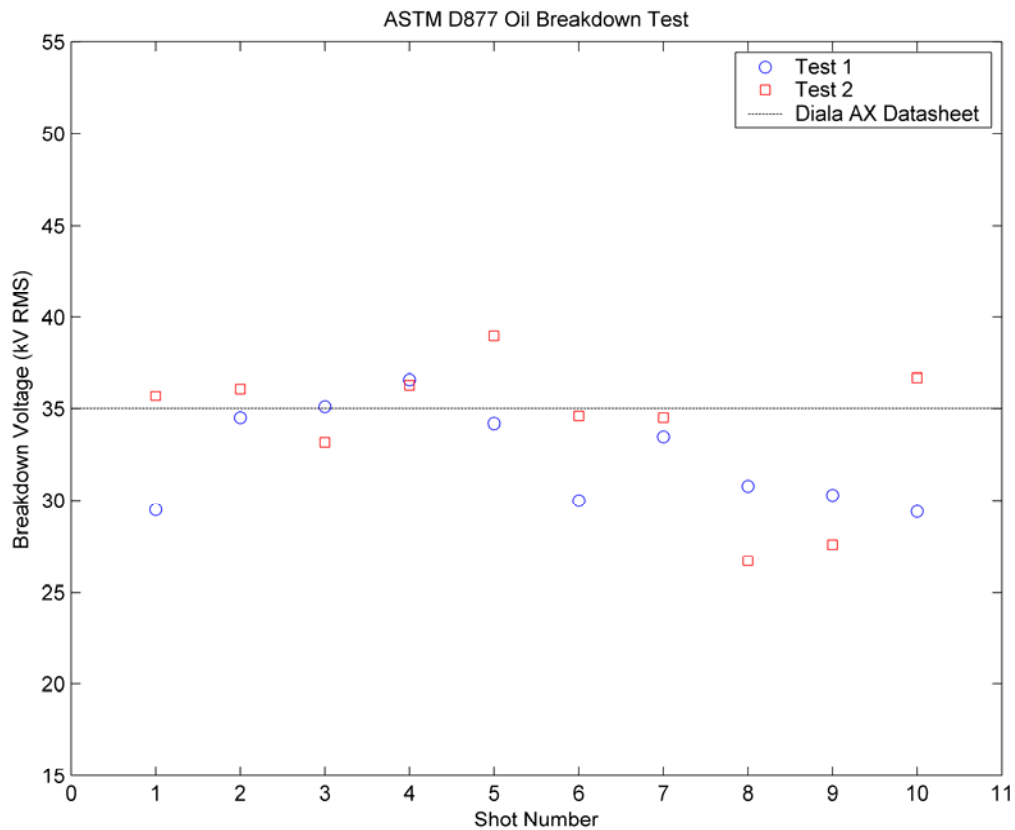


Figure 5.8. Oil breakdown with Hipotronics tester

It appears from the results of the ASTM D877 standard [6] breakdown test that the oil may be minimally saturated with water. The oil in the Marx tank is exposed to the atmosphere while the Marx is in operation. After operation, the oil is pumped out to the sealed, secondary storage tank, but the opportunity for water to infiltrate the oil exists when the Marx is in use. Water extraction can be attained though increased filtering.

References for Chapter 5

- [1] “Spiral delay line pulser: operation and maintenance manual”, Pulse Sciences, Inc., PSI-O&M-2420, Dec. 1991.
- [2] “Diala AX data sheet,” Shell Lubricants, [Online]. Available: <http://www.shell-lubricants.com/products/pdf/DialaA&AX.pdf>
- [3] J. C. Martin, “Nanosecond pulse techniques,” *Proceedings of the IEEE*, vol. 80, no. 6, pp. 934-945, Jun. 1992.
- [4] T. Martin, A. Guenther, and M. Kristiansen, Eds., *J. C. Martin on Pulsed Power*, New York: Plenum Press, 1996.
- [5] “OC60D Liquid dielectric test set,” Hipotronics, [Online]. Available: <http://www.hipotronics.com/pdf/OC6090D-DS0803.pdf>
- [6] “D877-02e1 Standard test method for dielectric breakdown voltage of insulating liquids using disk electrodes”, ASTM International, [Online]. Available: http://www.astm.org/cgi-bin/SoftCart.exe/DATABASE.CART/REDLINE_PAGES/D877.htm?L+mystore+xyx3815+1125378065

CHAPTER 6. ABRAMYAN NETWORK DESIGN

6.1. PFNs, PFLs, and the Abramyan Network

Desiring a rectangular pulse for a potential directed energy technology testbed with the UMC Marx in the most economical and space-conscious manner required a review of typical pulse-forming techniques. As introduced in Chapter 1, a pulse-forming line (PFL), or transmission line, lends itself to physical impracticalities due to excessive length requirements. In contrast, a pulse-forming network (PFN) may be smaller in size but more expensive due to specialty components. The third option is the implementation of an Abramyan network [1], [2], [3] into the current Marx configuration. Minimal addition of components is required thereby maximizing cost-efficiency and ease of installation.

For the required output parameters of approximately 1 MV for 1 μ s, PFLs, PFNs, and Abramyan networks all are reasonable methods of pulse shaping [4], [5], [6], [7]. As mentioned earlier, the sheer size of a PFL addition to the current configuration is a major concern. It is known that the duration of the output pulse is equal to twice the one-way transit time of the transmission line.

$$\tau_p = \frac{2l}{v_p} = 2\delta \quad (6.1)$$

$$v_p = \frac{c}{\sqrt{\epsilon_r}} \quad (6.2)$$

τ_p = duration of the pulse, s

l = length of line, m

- v_p = velocity of propagation, m/s
- δ = one-way transit time, s
- c = velocity of light, m/s
- ϵ_r = relative permittivity of dielectric, F/m

As Smith discusses in *Transient Electronics* [4], if a polymer plastic, like polypropylene, with a low dielectric constant ($\epsilon_r = 2-3$) is used as the dielectric, then the velocity of the pulse is approximately 2×10^8 m/s. This results in a transit time of about 20 cm/ns. To produce a 1 μ s pulse from this configuration would require 100 m of transmission line. This obviously violates the space constraints and is impractical for use with the UMC Marx. Additional disadvantages include the limited availability of impedances other than 50 Ω with the alternative of building a stripline of a different impedance both expensive and difficult.

PFNs are essentially lumped parameter approximations of PFLs and can require less space, but more specialized components. Using a Guillemin Type A PFN [4], [5] as an example, the required additional components are shown in Figure 6.1.

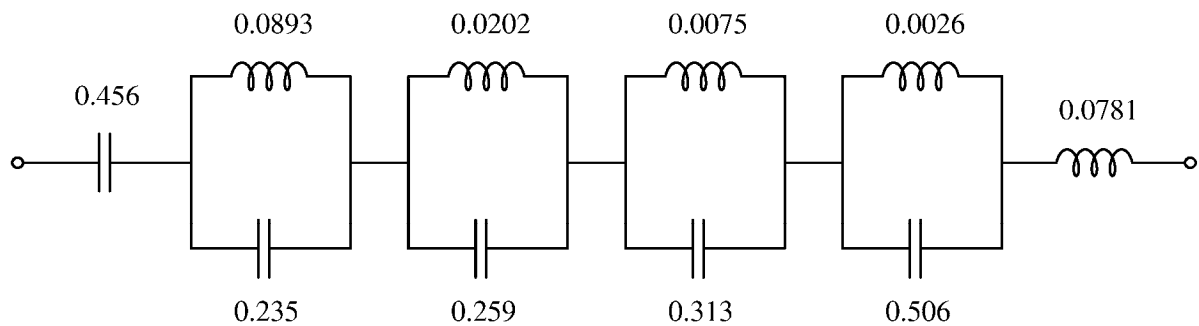


Figure 6.1. Guillemin Type A PFN [4], [5]

The values of the inductances for the network are calculated by multiplying the number supplied by the network impedance, Z_N , and the pulsewidth desired, τ . The values of the

capacitors are calculated by multiplying the number supplied by the pulsewidth and dividing by the impedance. As with any transmission line, or variant of, a matched load is always ideal. Therefore, $Z_N = 300 \Omega$ for the example. These parameters result in the PFN described in Figure 6.2.

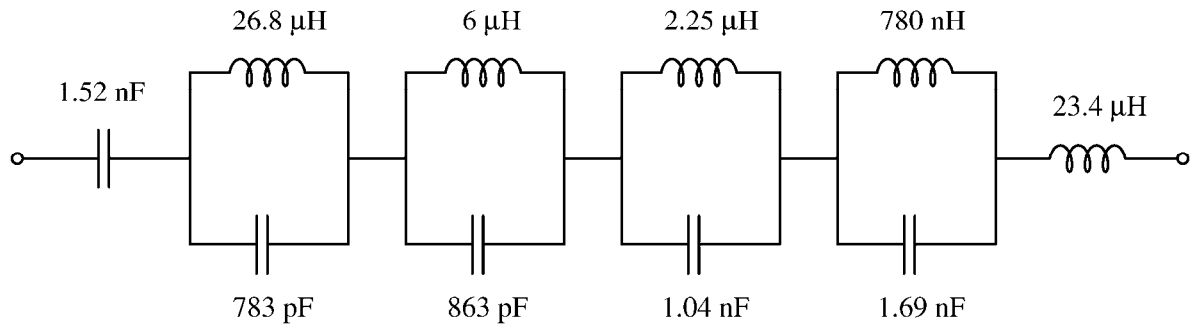


Figure 6.2. Type A PFN for UMC Marx

The values of the capacitors and inductors seem to encompass a large range. Although inductors can be wound differently for different inductances, capacitors are not nearly as adaptable. Compared to the pulse-forming line, this pulse shaping method results in the need for many additional components.

In contrast, the Abramyan network utilizes components readily available, and only requires the addition of a single, easy-to-construct inductor. The Abramyan network is simple to adjust for multiple output pulse requirements and can operate under the conditions of a collapsing load. Inductors of several values can be constructed for alternative parameters and can be interchanged in the system for varying pulse-forming needs. The Michigan Electron Long Beam Accelerator (MELBA) employed an Abramyan network to utilize the voltage compensation for a 1 μs collapsing diode load impedance [8], [9], [10], [11], [12], [13].

6.2. Physical Implementation of the Abramyan

Developing an Abramyan network for implementation in the UMC Marx began with an analysis of physical requirements. Ideally, all components should fit in the existing oil tank. To accomplish this, a few of the Marx stages must be removed. Testing of the Marx at 1 MV proved successful and therefore subtraction of stages from the 3 MV configuration is not a concern. Given that each stage is approximately 5 inches wide with supports, the removal of 5 stages provides approximately 2 more feet of length in the tank to utilize for other purposes. It is assumed this is enough space to fit an inductor in the tank given the calculations following (Equation 6.3 and Equation 6.4).

Applying a reasonable inductor value of 5 μH to the Wheeler formulas [14], [15] for inductance, basic geometry can be specified to determine the corresponding number of turns required. With the use of 1.27cm (0.5 in) bendable copper pipe, a coil diameter of 30.48 cm (12 in) and coil length of 30.48 cm (12 in) appears to be reasonable. The Wheeler formula determines that 5 turns are necessary to reach a 5 μH inductance.

$$L = \frac{d^2 \cdot n^2}{l + 0.45 \cdot d} \quad (6.3)$$

L = inductance (μH), 5.26

d = coil diameter (m), 0.3048

l = coil length (m), 0.3048

n = number of turns, 5

The next step in the inductor design is to verify that the electric field strength between the coils is not greater than the breakdown strength of the transformer oil. The coil radius, spacing, and voltage between coils can be used with the Bouwers and Cath maximum field strength formula for two cylinders [16]. Observing a conservative transformer oil breakdown

strength of 40 kV/cm [17], the resultant electric field strength of 26 kV/cm is well within the limits of safe operation. Therefore, the space allocated for the inductor is sufficient.

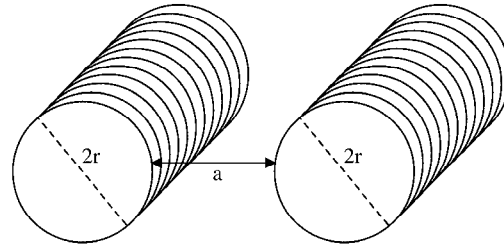


Figure 6.3. Two cylinders (approximating turns of copper pipe)

$$E_{\max} = 0.9 \cdot \frac{V/2}{2.3 \cdot r \cdot \log\left(\frac{r + a/2}{r}\right)} \quad (6.4)$$

- E_{\max} = maximum electric field, 26 kV/cm
- V = potential difference between coils, 90 kV
- a = coil spacing, 6.096 cm (12in / 5turns = 2.4 in)
- r = coil radius, 1.27 cm (0.5 in)

It was also desired to have a small amount of room in the tank to slightly separate the reverse-charging stages from the forward-charging stages. An additional 3 stages were allocated for removal for this purpose. A total of 8 stages are then designated removable. The remaining 22 stages will need to be optimized in the Abramyan network configuration. The original 3 MV Marx configuration from Figure 2.2 can be adjusted with the removal of stages and simplified to the circuit in Figure 6.4.

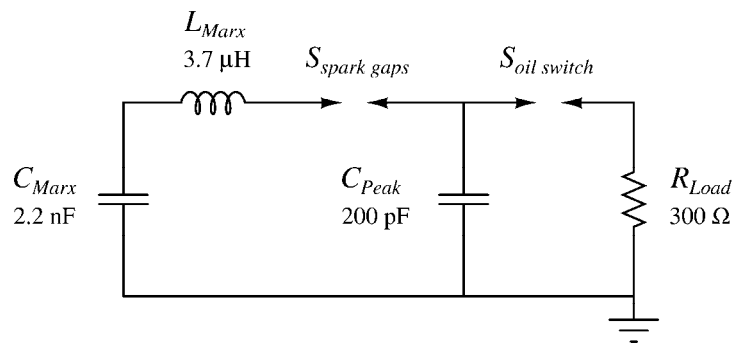


Figure 6.4. Equivalent Marx circuit with twenty-two stages

Implementing the Abramyan network into the above circuit results in the schematic shown in Figure 6.5. Values are not listed for C_{Marx} and L_{Marx} due to recalculations needed based on the reallocation of stages for C_a and L_a . These calculations will occur in the following section.

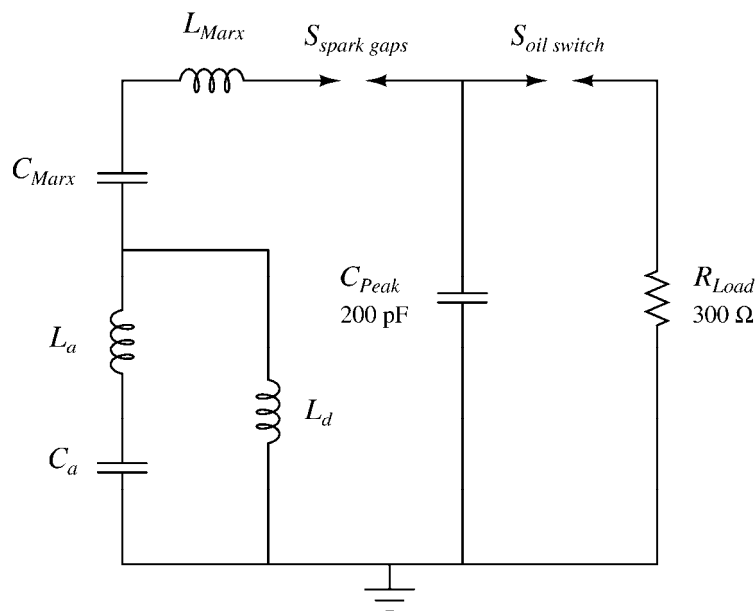


Figure 6.5. Basic Abramyan in twenty-two stage Marx

This circuit can be implemented in the UMC Marx with minimal cost. Simulations were conducted with the removal of eight stages for a total of twenty-two functioning stages. Optimizing this circuit for a 1 MV output with a 1 μ s pulsewidth, a total of five stages were reverse-charged in the simulations. Determining the number of stages to be reversed is based on the desired output voltage. The output of the Marx with the Abramyan is the result of subtracting the voltage on reverse-charged stages from the voltage on the forward-charged stages. All capacitors were charged to 90 kV (+50 kV, -40 kV) per stage to match the current power supplies in the system. The equivalent capacitance of the reversed stages is 9.6 nF. At 90 kV per stage charge, the reverse-stage capacitors will charge to a total voltage of -450 kV. The series inductance of these capacitors is 766.7 nH. The remaining stages constitute an equivalent capacitance of 2.8 nF with a series inductance of 2.6 μ H. The charge on these stages at 90 kV per stage is 1.53 MV. The peak expected output from the Marx and Abramyan with the reversal of 5 stages is 1.08 MV (forward 1.53 MV – reverse 450 kV).

6.3. Circuit Simulations

The challenge in Abramyan network design is the optimization of the additional inductor, L_d . By its nature, the design of an Abramyan network is an iterative process of determining possible solutions and realizable components [18]. One method of analysis is to approach the Abramyan as the addition of a simple oscillating tank circuit. A tank circuit consists of a capacitor and inductor in parallel with a resonant frequency f_r .

$$f_r = \frac{1}{2\pi\sqrt{LC}} \quad (6.5)$$

With the selection of five reverse-charged stages, the capacitance C_a and inductance L_a of the reverse-charged stages maintain fixed values of 9.6 nF and 766.7 nH respectively. The only remaining variable is the additional inductor, L_d . Because L_a and L_d can be assumed to be in series, the sum of the two will serve as the total parallel inductance of the tank circuit. Choosing $L_d = 5\mu\text{H}$ results in the following calculations.

$$f_r = \frac{1}{2\pi\sqrt{5.7667\mu\text{H} \cdot 9.6\text{nF}}} = 676\text{kHz} \quad (6.6)$$

$$T_r = \frac{1}{f_r} = \frac{1}{676\text{kHz}} = 1.5\mu\text{s} \quad (6.7)$$

The period calculated is 150% of the pulse length desired from the output of the Marx and Abramyan circuit. This result can be used for a variety of inductor values to determine approximate pulse length (Table 6.1). These values can be verified by the simulation results in Figure 6.6 and Figure 6.7. The slight increase or decrease in inductor values as described above facilitate changes in both the pulse width and amplitude to suit many output specifications.

Table 6.1. Expected pulse lengths from variable inductor values

Inductor value	Expected pulse length
1 μH	546 ns
3 μH	798 ns
5 μH	986 ns
7 μH	1.14 μs
9 μH	1.28 μs

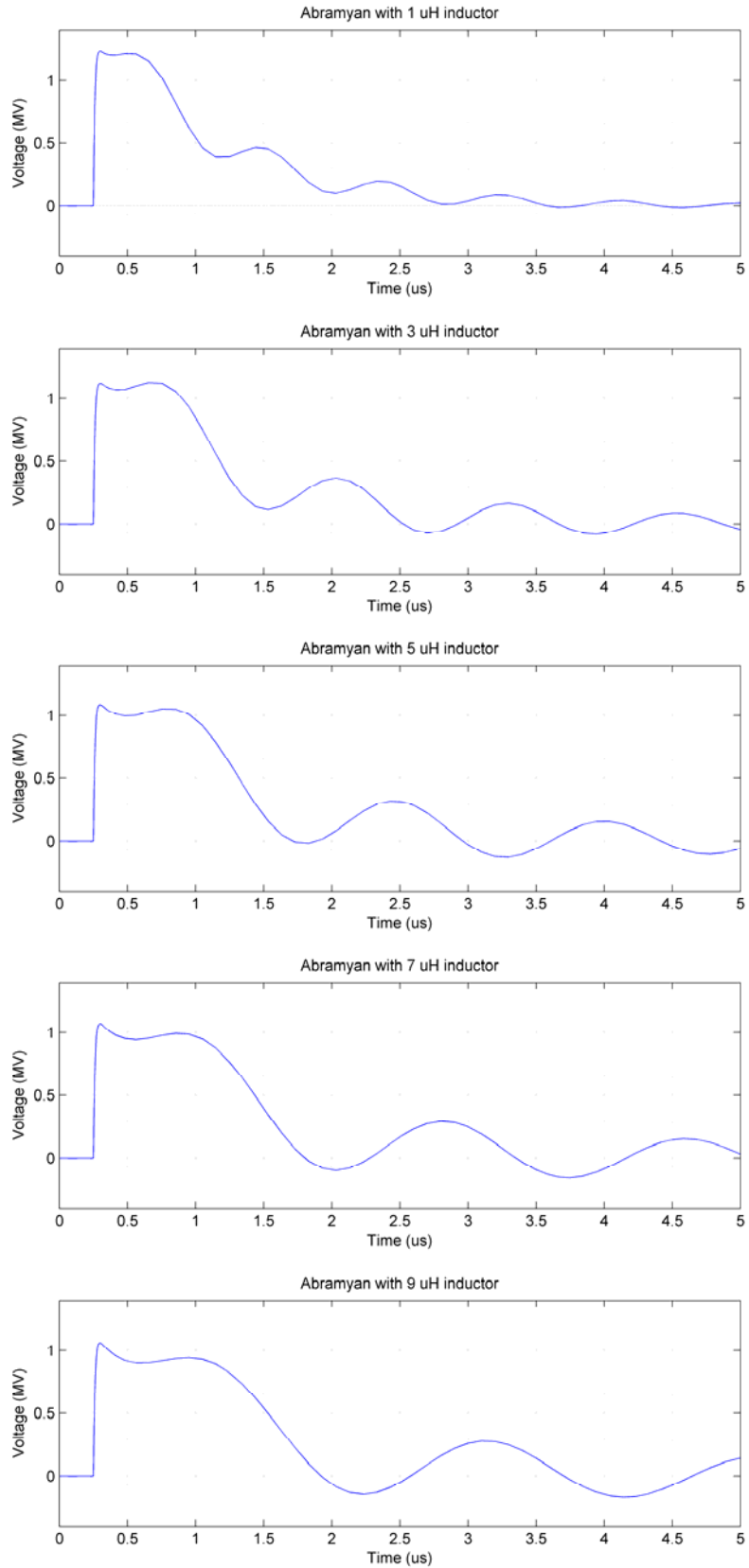


Figure 6.6. Abramyan network with inductor values 1 μH - 9 μH

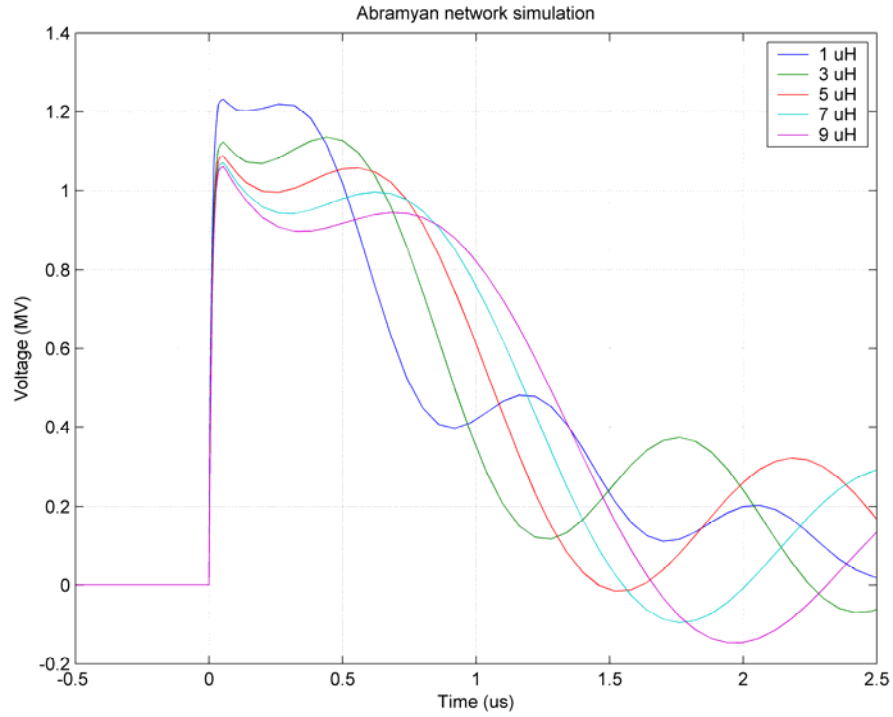


Figure 6.7. Varying Abramyan network inductor values

Additionally, previous work at Pulse Sciences, Inc. [18] indicates a correlation between the frequency of the reversal stage and the rate of change of voltage on the reversal stage $V_R(t)$ at the zero crossing point. This relationship is given by [18]:

$$\frac{dV_R(t)}{dt} = \frac{V_a}{\sqrt{(L_a + L_d) \cdot C_a}} \quad (6.8)$$

assuming

$$(R_a + R_d) \ll \sqrt{\frac{(L_a + L_d)}{C_a}} \quad (6.9)$$

The load voltage droop is given by

$$\frac{dV_L}{dt} = \frac{I_L}{C_e} = \frac{V_L}{R_L \cdot C_e} \quad (6.10)$$

where $C_e = C_a \parallel C_m$ [18]. Following the derivation in this reference, Equation 6.10 can be set to equal Equation 6.8 to solve for C_e . Since C_e is a known variable in our situation, this equation can be used to solve for L_d . The previous equations are combined and give Equation 6.11.

$$L_d = \frac{V_a^2 \cdot R_L^2 \cdot C_e^2}{V_L^2 \cdot C_a} - L_a \quad (6.11)$$

This equation was utilized in a MATLAB program to quickly calculate values for a variety of parameters. The code is documented with sample output in Appendix E. The output of the program gives a range of values for L_d that are optimized for output voltages between 1 - 1.5 MV and apply to the selected input parameters. The ranges supplied can be simulated in PSPICE to determine the optimum value for the desired pulse shape.

The previous sets of calculations also show correlation with the plot from the Laplace transform developed in Mathematica in Figure 6.8 [19], [20]. This graph represents the signal components (red, blue, and green) that together compose the output pulse (dashed purple). The green line represents the forward-charged capacitors, the red line represents the reverse-charged capacitors, and the blue line represents the ringing of the Abramyan circuit. With an oscillation period of 1.5 μs , the highest voltage peak of the ringing circuit occurs at $0.5T_r$, shown by the blue line. Therefore, the peak voltage from the Abramyan or tank circuit would occur at 750 ns. The voltage remaining on the forward-charged capacitors shown in green is approximately 50% at this time. This appears to be the ideal combination for the parameters and output required. Full documentation of the Mathematica code developed to calculate this plot is provided in Appendix F.

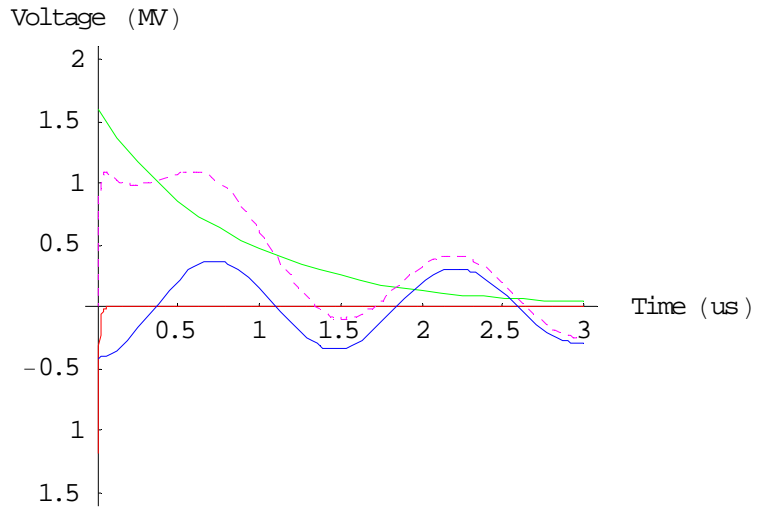


Figure 6.8. Signal decomposition of Abramyan with Marx

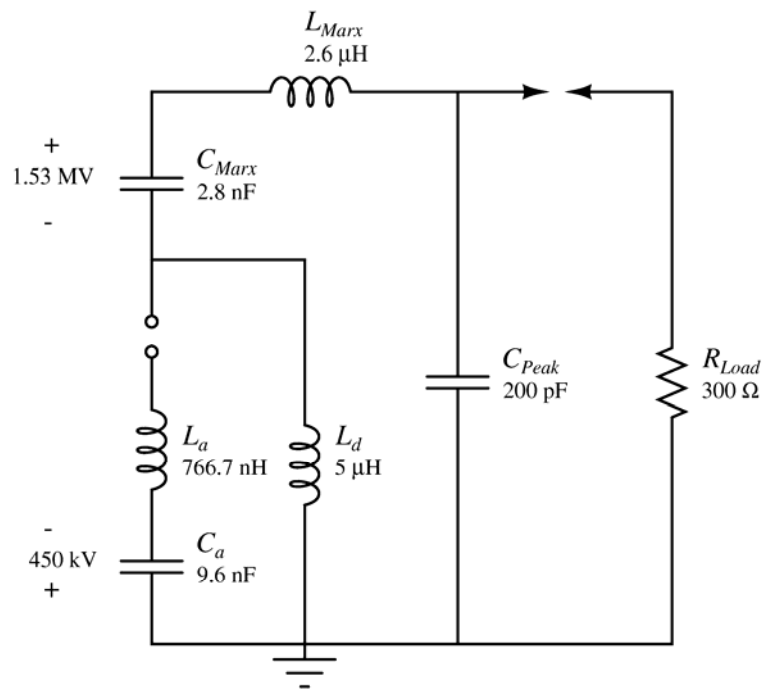


Figure 6.9. Conceptual design of UMC Marx with Abramyan network

For the pulse specification proposed, it appears that the selection of a $5 \mu\text{H}$ inductor is appropriate. Further PSPICE simulations were conducted on the circuit in Figure 6.9.

Simulation code is documented in Appendix G. The resultant pulse is seen in Figure 6.10 with the characteristics listed in Table 6.2. The risetime of the pulse increased minimally from the original Marx configuration while the pulse width increased dramatically.

Table 6.2. Abramyan network pulse characteristics, $L_d = 5 \mu\text{H}$

Risetime (10-90%)	24 ns
Pulse width (90-90%)	0.8 μs
Fall time (10-90%)	0.5 μs
Pulse-top ripple	$\pm 8\%$

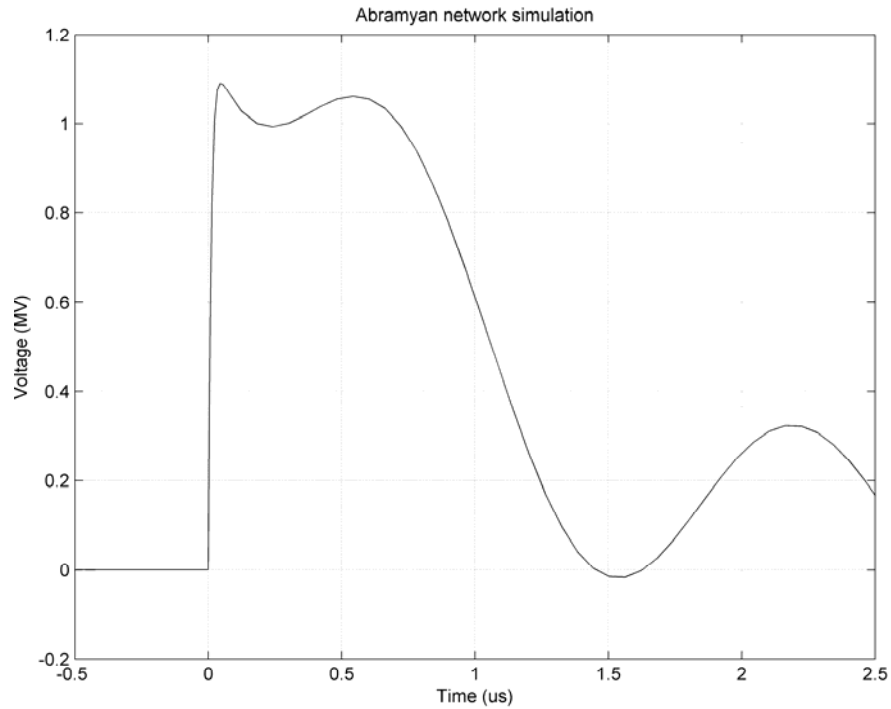


Figure 6.10. Marx and Abramyan with 5 μH inductor

Simulations were also conducted to test the possibility of triggering the spark gap switches at different times and the results indicated no advantage. Triggering the switches at the same time, or without modification, appeared to optimize the pulse.

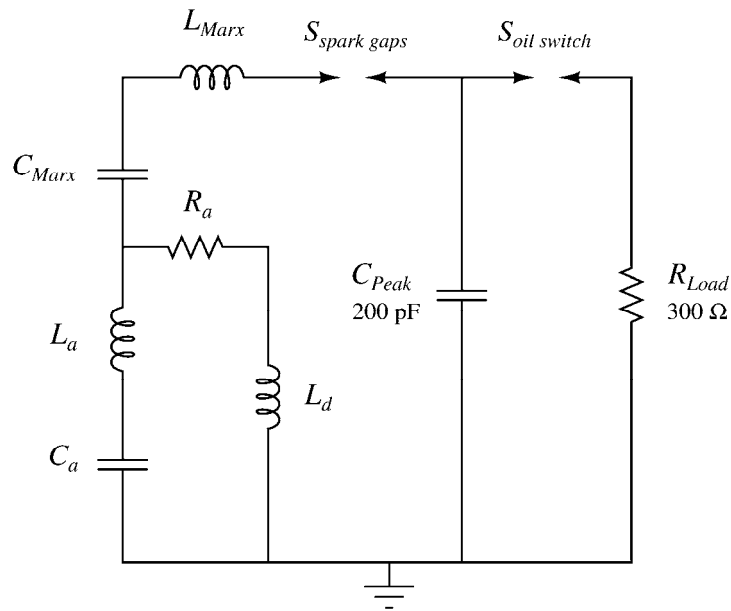


Figure 6.11. Abramyan with damping resistor

The drawback to the Abramyan network is the voltage reversal on the reverse-charged stages. Damping resistors can be placed in the Abramyan section of the circuit in Figure 6.11 to reduce the ringing seen in Figure 6.12 but accompany a decrease in pulse width in Figure 6.13 and Table 6.3. The ringing circuit that reverses the charge on the capacitors is also responsible for the pulse extension.

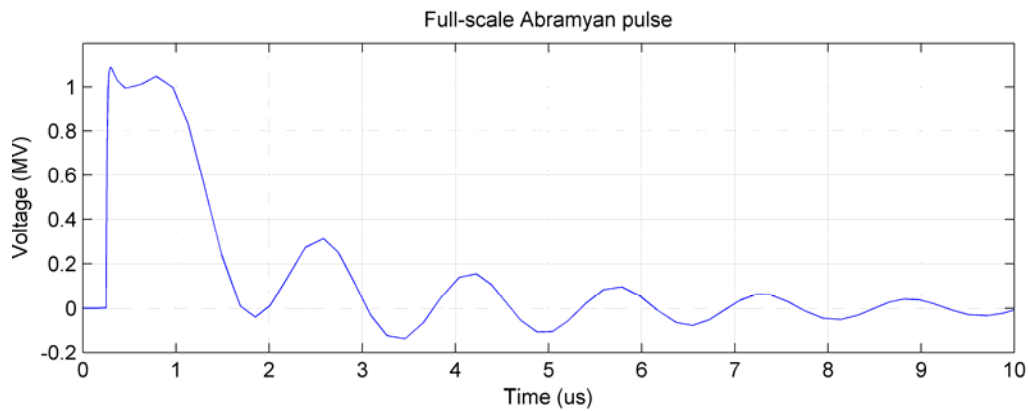


Figure 6.12. Full length output from Abramyan and Marx

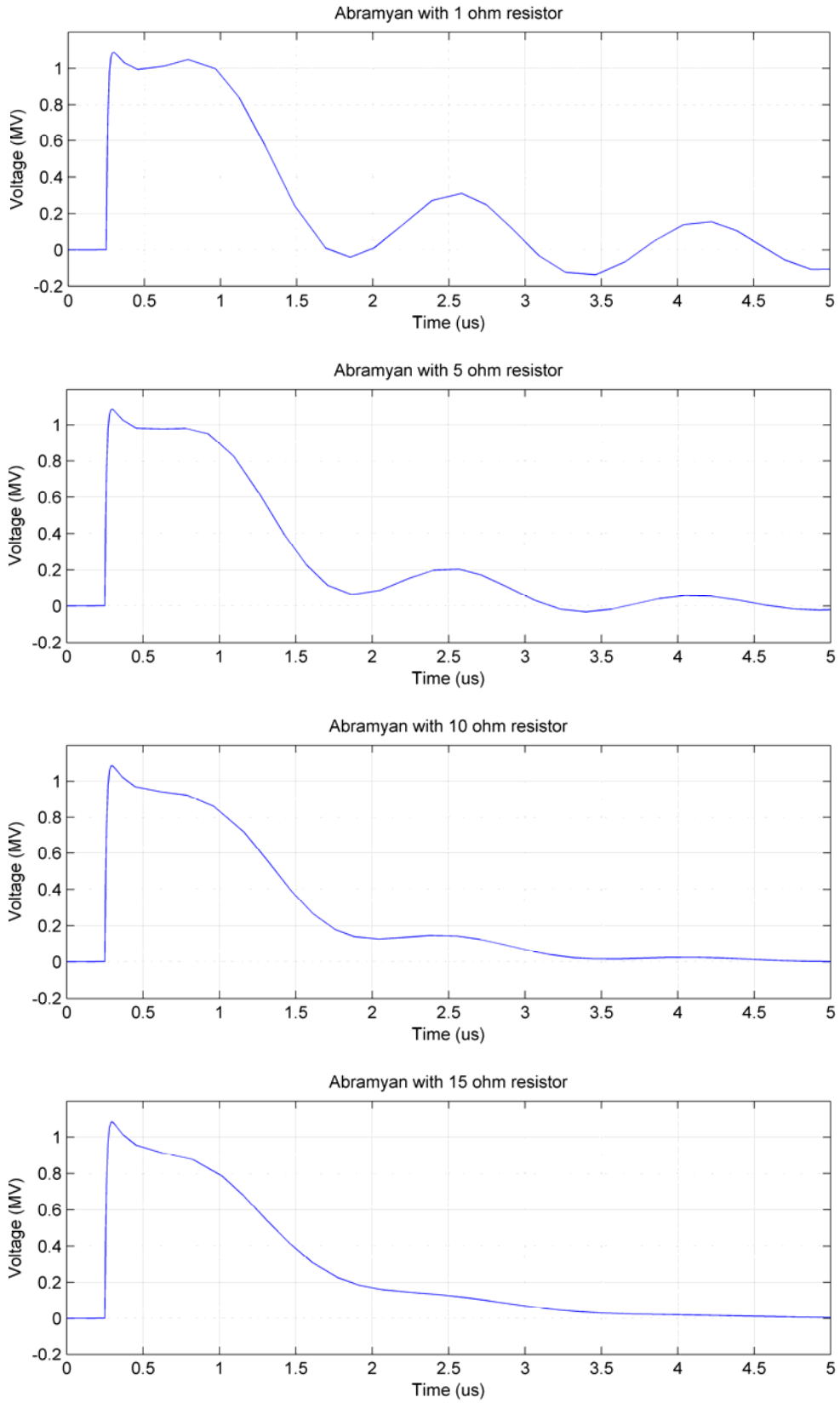


Figure 6.13. Output pulses with damping resistor in the 5 μH Abramyan network

Table 6.3. Pulse lengths for resistance values in Abramyan

Resistance value	Pulse length (90-90%)
1 Ω	800 ns
5 Ω	720 ns
10 Ω	580 ns
15 Ω	410 ns

The decrease in pulse width is attributed to the same resistor that damps the late-time ringing of the pulse. From the plots in Figure 6.13, the optimum resistance value to supplement the UMC Abramyan appears to be between 1 and 5 Ω . The late-time ringing is damped in approximately three periods while decreasing pulse width by only 80 ns. This is a significant portion of the 800 ns pulse, but the long-term benefit of increasing capacitor lifetime may outweigh the alternative.

Another possible solution was employed on MELBA [8], [9], [10], [11], [12], [13]. The circuit contained a high pressure crowbar switch that was triggered to remove 90% of the generator voltage in approximately 40 ns [8]. With this option, smaller resistance values can be used if the crowbar terminates the pulse before the late-time ringing can occur. Additionally, the introduction of time-variable resistance into the Abramyan stage presents many potential possibilities.

Keeping in mind that the Abramyan network utilizes components already available and only requires the addition of a single component, the drawbacks discussed can be seen as a minor compromise to its ease of construction. While some capacitor reversal is inherent in a circuit of this type, the simplicity of the Abramyan network addition to operational systems provides a cost-effective solution to the requirement of a rectangular pulse.

References for Chapter 6

- [1] E. A. Abramyan, E. N. Efimov, and G. D. Kuleshov, "Correction of the pulse shape of an Arkad'ev-Marks voltage generator," High-Temperature Institute of the Academy of Sciences of the USSR, Moscow. Translated from *Pribory i Tekhnika Éksperimenta*, No. 4, pp.170-172, Jul.-Aug. 1979.
- [2] E. A. Abramyan, B. A. Altercorp, and G. D. Kuleshov, "Microsecond intensive e-beams", *Proceedings of the 2nd International Topical Conference on Power Electron and Ion Beam Research and Technology*, pp. 743-754, Oct. 1977.
- [3] E. A. Abramyan, E. N. Efimov, and G. D. Kuleshov, "Energy recovery and power stabilization of pulsed electron beams in Marx generator circuits", *Proceedings of the 2nd International Topical Conference on Power Electron and Ion Beam Research and Technology*, pp. 755-760, Oct. 1977.
- [4] P. W. Smith, *Transient Electronics: Pulsed Circuit Technology*, Wiley, 2002.
- [5] G. N. Glasoe and J. V. Lebacqz, Eds., "Pulse Generators", *Massachusetts Institute of Technology Radiation Laboratory Series*, McGraw-Hill, 1948.
- [6] S. T. Pai and Q. Zhang, *Introduction to High Power Pulse Technology*, World Scientific, 1995.
- [7] I. Smith, "Pulsed power for 0.3-0.5 μ s durations", *Lawrence Livermore National Laboratory Report*, 18318, Oct. 1979.
- [8] R. M. Gilgenbach, L. D. Horton, R. F. Lucey, Jr, S. Bidwell, M. Cuneo, J. Miller, and L. Smutek, "Microsecond electron beam diode closure experiments", *Proceedings of the 5th IEEE Pulsed Power Conference*, pp. 126-132, Jun. 1985.

- [9] J. I. Rintamaki, "Effects of RF plasma processing on the impedance and electron emission characteristics of a MV beam diode", Doctoral dissertation, University of Michigan, 1999.
- [10] J. M. Hochman, "Microwave emission of large and small orbit rectangular gyrotron devices", Doctoral dissertation, University of Michigan, 1998.
- [11] M. T. Walter, "Effects of tapering on high current, long pulse gyrotron backward wave oscillator experiments", Doctoral dissertation, University of Michigan, 1995.
- [12] M. E. Cuneo, "Characterization of the time-evolution of a microsecond electron beam diode with anode effects", Doctoral dissertation, University of Michigan, 1989.
- [13] M. E. Cuneo, "Spectroscopic study of anode plasmas in a microsecond electron beam diode", *IEEE Transactions on Plasma Science*, vol. 15, no. 4, pp. 375-379, Aug. 1987.
- [14] H. A. Wheeler, "Formulas for the skin effect," Proceedings of the I.R.E., pp 412-424, Sept. 1942.
- [15] H. A. Wheeler, "Simple inductance formulas for radio coils," Proceedings of the I.R.E., pp 1398-1400, Oct. 1928.
- [16] A. Bouwers and P. G. Cath, "The maximum electric field strength for several simple electrode configurations," *Philips Tech. Review*, vol. 6, no. 9, pp. 270-278, 1941.
- [17] R. J. Adler, "Pulse power formulary," North Star Research Corporation, [Online]. Available: <http://www.northstar-research.com/PDF/Formweb1.pdf>
- [18] R. Curry, K. Nielsen, I. Smith, "Abramyan networks: a general purpose network for linear induction accelerators", Pulse Sciences, Inc., San Leandro, CA, Apr. 1986.
- [19] G. V. Lago and D. L. Waidelich, *Transients in Electrical Circuits*, New York: Ronald Press, 1958.
- [20] Mathematica 4.1 for Students [Online]. Available: www.mathematica.com

CHAPTER 7. CONCLUSION

This thesis has presented the development of the large-gap oil dielectric switch test facility at the University of Missouri-Columbia. Designs for future Abramyan network implementation have been included in this work. A description of the system for all future research on the UMC Marx is documented and thoroughly explained. The simulation circuits and code have been developed and accurately predicted experimental results. Early test data has proven the Marx to reliably operate at the desired 1 MV output with capability for increased output voltages up to 3 MV. Abramyan network designs for multiple output ranges are available for implementation.

Chapter 1 provided an introduction to Marx generators and the need for pulse shaping systems. Basic Marx circuits were developed and analyzed. Abramyan networks were introduced with the possibility of implementation into the UMC Marx generator.

The UMC Marx facility was described in detail in Chapter 2. Enhanced circuits with detailed parameters were determined. The subsystems of the Marx including the charging system, the triggering system, and the peaking switch were discussed relative to the control system.

Diagnostics for the facility were developed in Chapter 3. Voltage divider theory was discussed and applied to the UMC Marx. Construction and calibration of the dividers was also mentioned. Testing of the dividers proved successful and resulted in implementation into the Marx system.

The UMC Marx was modeled and simulated in Chapter 4. Simulations of the Marx circuits produced expected results. Breakdown of the output switch was calculated for use with variable gap spacing and charge voltage in experimental work. Electrostatic simulations were

conducted to analyze the electric fields present with the geometry of the output switch. The electric field calculations and electrostatic simulations provided similar results. From the maximum field strengths determined, the field enhancement factor was calculated and proved reasonable in the following chapter.

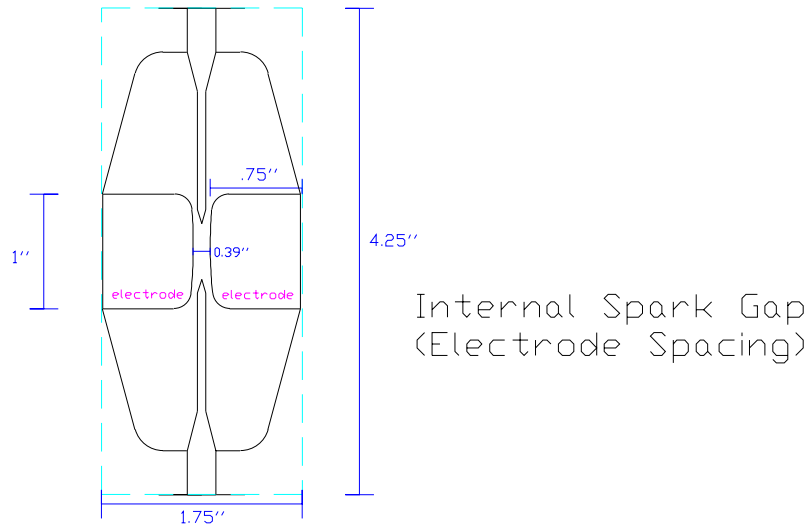
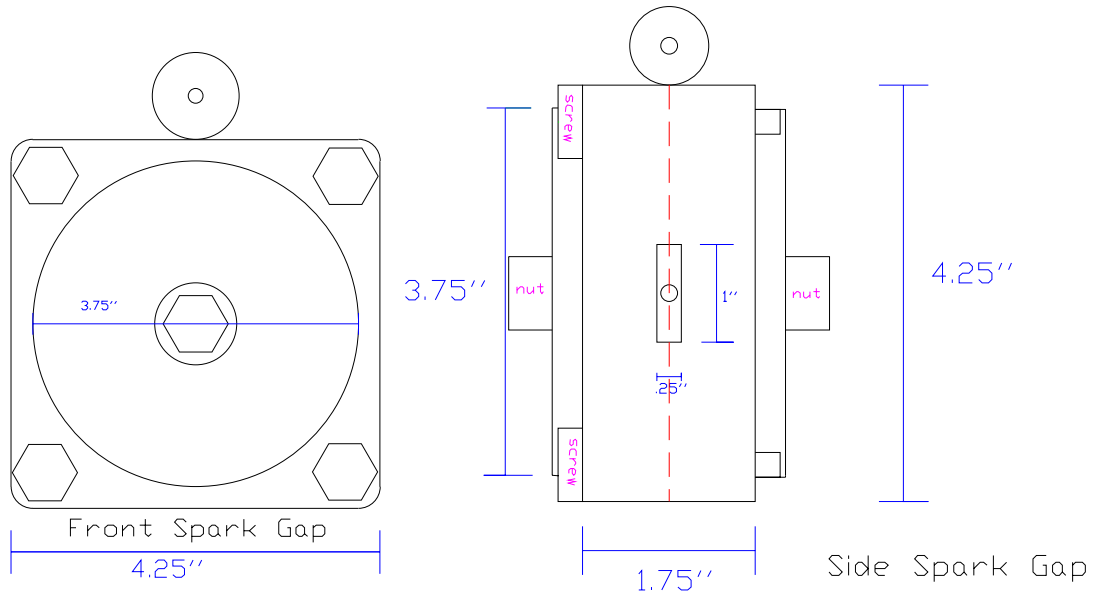
Chapter 5 provided experimental parameters and results. The Marx performed as expected under 1 MV operation. Operation at higher voltages may require modifications to the output switch geometry. The increased electric fields on the field shaper appeared to affect the pulse after successive shots with minimal carbon filtration. Industry standard oil breakdown tests indicated the possibility of water saturation. Both carbon and water accumulation in the oil can be addressed with enhanced filtering capabilities.

An Abramyan network was designed for the UMC Marx in Chapter 6. Background information on the alternative pulse-forming lines and pulse-forming networks was presented. Designs of the physical implementation into the Marx were discussed and simulations of expected output followed.

Future work includes further studies in oil breakdown and specific levels of impurities in the oil. It may also be determined that a threshold level of carbon exists allowing the Marx to maintain a repeatable result such as in Figure 5.7. Additionally, the output polarity of the Marx can be reversed for further oil switch testing.

At the conclusion of this project, the UMC Marx is now operational and oil switch testing is currently being conducted. Conceptual Abramyan network designs for the UMC Marx have been optimized to deliver a 1 μ s pulse at 1 MV and are available for implementation.

APPENDIX A. SPARK GAP DIMENSIONS



APPENDIX B. MARX SIMULATION CODE

This code was developed from PSPICE schematics to simulate the Marx parameters both with and without the peaking circuit. Results from these simulations are discussed in Chapter 4. The first section describes the Marx circuit without the peaking capacitor. The second section includes the peaking capacitor in the analysis of the circuit.

```
*Libraries:
* Local Libraries :
* From [PSPICE NETLIST] section of pspice91.ini file:
.lib "nom.lib"

*Analysis directives:
.TRAN 0 2u 0 1ns
.PROBE
.INC "simple marx-SCHEMATIC1.net"

**** INCLUDING "simple marx-SCHEMATIC1.net" ****
* source SIMPLE MARX
C_C1          0 N00016  1.6n IC=-3MEG
L_L1          N00116 N00022  4.6u
R_R1          0 N00022  300
X_U1          N00016 N00116 Sw_tClose PARAMS: tClose=.399u
ttran=1n Rclosed=0.01
+ Ropen=1Meg

**** INCLUDING "simple marx-SCHEMATIC1.als" ****
.ALIASES
C_C1          C1(1=0 2=N00016 )
L_L1          L1(1=N00116 2=N00022 )
R_R1          R1(1=0 2=N00022 )
X_U1          U1(1=N00016 2=N00116 )
.ENDALIASES

.END
```

```

****      Voltage Controlled Switch MODEL PARAMETERS
*****

```

```

          X_U1.Smod
      RON      .01
      ROFF     1.000000E+06
      VON      1
      VOFF     0

```

```

****      INITIAL TRANSIENT SOLUTION
TEMPERATURE = 27.000 DEG C
*****

```

```

NODE   VOLTAGE      NODE   VOLTAGE      NODE   VOLTAGE      NODE
VOLTAGE

(N00016) 3.000E+06 (N00022) 899.7300 (N00116) 899.7300
(X_U1.3) 0.0000

```

```

VOLTAGE SOURCE CURRENTS
NAME          CURRENT

X_U1.V1      0.000E+00

```

```

TOTAL POWER DISSIPATION 0.00E+00 WATTS

```

```

JOB CONCLUDED

```

```

TOTAL JOB TIME .19

```

The following is from the Marx schematic including the peaking switch.

```

*Libraries:
* Local Libraries :
* From [PSPICE NETLIST] section of pspice91.ini file:
.lib "nom.lib"

```

```

*Analysis directives:
.TRAN 0 2u 0
.PROBE
.INC "marx-SCHEMATIC1.net"

```

```

**** INCLUDING marx-SCHEMATIC1.net ****
* source MARX
C_Cm          N00009 0 1.6nF IC=1.02MEGV
L_Lm          N03740 N00015 4.6uH IC=0
R_R           0 N00017 300
C_C3          0 N00015 200p IC=0
X_U4          N00015 N00017 Sw_tClose PARAMS: tClose=399ns
ttran=0 Rclosed=0.01
+ Ropen=1Meg
X_U2          N00009 N03740 Sw_tClose PARAMS: tClose=350ns
ttran=0 Rclosed=0.01
+ Ropen=1Meg

```

```

**** RESUMING marx-schematic1-marxsim.sim.cir ****
.INC "marx-SCHEMATIC1.als"

```

```

**** INCLUDING marx-SCHEMATIC1.als ****
.ALIASES
C_Cm          Cm(1=N00009 2=0 )
L_Lm          Lm(1=N03740 2=N00015 )
R_R           R(1=0 2=N00017 )
C_C3          C3(1=0 2=N00015 )
X_U4          U4(1=N00015 2=N00017 )
X_U2          U2(1=N00009 2=N03740 )
.ENDALIASES

```

```

**** RESUMING marx-schematic1-marxsim.sim.cir ****
.END

```

```

**** Voltage Controlled Switch MODEL PARAMETERS
*****

```

	X_U4.Smod	X_U2.Smod
RON	.01	.01
ROFF	1.000000E+06	1.000000E+06
VON	1	1
VOFF	0	0

```

**** INITIAL TRANSIENT SOLUTION
TEMPERATURE = 27.000 DEG C
*****

```

```

NODE VOLTAGE NODE VOLTAGE NODE VOLTAGE NODE
VOLTAGE

```


(N00009) 1.020E+06 (N00015) 2.038E-06 (N00017) 611.2E-12
(N03740) 1.019E+06

(X_U2.3) 0.0000 (X_U4.3) 0.0000

VOLTAGE SOURCE CURRENTS
NAME CURRENT

X_U4.V1 0.000E+00
X_U2.V1 0.000E+00

TOTAL POWER DISSIPATION 0.00E+00 WATTS

JOB CONCLUDED

TOTAL JOB TIME .98

APPENDIX C. MARX OPERATION

Preparation for Marx Operation

- 1 Determine Marx charge voltage, _____ kV per power supply.
- 2 From Figure 4.2 in *Spiral Delay Line Pulser Manual*, determine Marx spark gap operating pressure, _____ psig.
- 3 From Figure 4.3, determine oil switch gap spacing, _____ cm.
- 4 Determine trigger generator charge voltage, _____ kV.
- 5 From Figure 4.1, determine trigger generator operating pressure, _____ psig.
- 6 Verify intended charge polarity is consistent with Marx input charge lines.
 - Positive output = Positive charge to first capacitor, negative to second.
 - Negative output = Negative charge to first capacitor, positive to second.
- 7 Slightly pressurize spark gaps (5-10 psi) to discourage oil leaking into them.
- 8 Verify all resistors and gas lines are correctly installed.
- 9 Check all connections at low voltage end of Marx are secure. Pay special attention to trigger lines into resistor connection balls.
- 10 Plug in both power cables to hydraulic pump.
 - Control box cable
 - Pump cable
- 11 Turn on pump and raise Marx slightly to remove safety pins.
- 12 Remove all 4 safety pins.
- 13 Lower Marx into tank.
- 14 Check Marx top frame is sitting on current contacts on both low and high voltage ends of tank.
- 15 Turn hydraulic pump off.
- 16 Unplug both pump power cables (control and pump).
- 17 Set oil switch spacing to distance determined in **Step 3**.
- 18 Clear area and move scaffolding away from tank.
- 19 Open valves to oil wash recirculator pump. Turn on pump.
- 20 Verify safety ground connections from trigger generator, control/charging cabinet, and tank to wall.
- 21 Open window and secure both SF₆ and air vents outside.
- 22 Pressurize pneumatic cylinders with air to 95 psig. (Do not exceed 100 psi - Versa valve maximum.)
- 23 Plug isolation transformer into wall.
- 24 Turn transformer on.
- 25 Check all 4 plugs in control/charging cabinet power strip.
- 26 Turn on control/charging cabinet power strip.
- 27 Pressurize Marx spark gaps with SF₆ to pressure determined in **Step 2**.
- 28 Pressurize trigger generator with SF₆ to pressure determined in **Step 5**. (Purging need only be done one every 15 shots.)
- 29 Verify output circuit configuration with associated monitor connections.
- 30 Set up barriers around test area.

Operating Procedure

Verify scope is ready for output data

- 31 Turn off oil wash recirculating pump.
- 32 Turn CONTROL POWER ENABLE KEY to turn control panel on.
- 33 Manually depress the DUMP button to clear controller of any abnormal start-up logic states.
- 34 Check the trigger charge rate (pot on back of cabinet). It should be set to track slightly ahead of desired Marx charge level.
- 35 Set the pot on each Marx power supply to zero.
- 36 Verify all interlocks are satisfied.
- 37 Evacuate test area.
- 38 Announce start **Pre-charge Sequence**.
- 39 Push CHARGE button.
- 40 Slowly increase voltage on both Marx power supplies to set the voltage to the correct charge level for firing.
- 41 Turn off Marx power supplies and hit DUMP. The Marx is now ready for the firing sequence.
- 42 Announce start **Firing Sequence**.
- 43 Follow the numbered-button firing procedure on the control cabinet.
 - Charge button
 - 80kV Glassman power on
 - 50kV Glassman power on
 - -40kV Kaiser power on
- 44 Monitor charge sequence on control panel. Sequence can be terminated at any time by pushing DUMP button.
- 45 When FIRE light turns RED the system can be triggered by pushing the FIRE button.

- **46** Follow the numbered-button **Turn-off Procedure** on the control cabinet. ****Be sure to begin this immediately after Marx fires****
 - -40kV Kaiser power off
 - 50kV Glassman power off
 - 80kV Glassman power off
 - Control power enable off
- **47** Manually depress DUMP switch after each shot as an additional safety precaution.

Shutdown Procedure

Short-term:

- **48** Set the pressure in the spark gaps to 10 psig.
- **49** Set the pressure in the trigger vessel to 10 psig.
- **50** Turn off the CONTROL POWER ENABLE KEY.
- **51** Close valves in the compressed air supply line.
- **52** Close valves on SF₆ cylinder and in supply line.
- **53** Close valves on oil recirculating pump.
- **54** Remove barriers around test area.

Long-term:

- **55** For extended shutdown periods, the system should be drained of oil. Prior to startup the Marx should be carefully inspected.

APPENDIX D. MARX SHOT LOG

Date	Shot #	Marx Charge Voltage (\pm kV)	Spark Gap Pressure (psi)	Trigger Charge Voltage (kV)	Trigger Gen Pressure (psi)	Gap Spacing (dial reading)	Ch.1 File #	Ch. 2 File #	Notes
3/17/2005	1	17	4	40	15	180	-	-	trigger generator pre-breaking, need to increase TG pressure
3/17/2005	2	17	4	40	20	180	0	1	arcing to ground at output, data appears as rectangular pulse
3/17/2005	3	20	4	40	20	160	2	3	decreasing gap spacing
3/17/2005	4	20	4	40	20	140	4	5	
3/17/2005	5	20	4	40	20	190	6	7	
3/17/2005	6	20	4	40	20	190	8	9	flushed carbon away from electrode
3/17/2005	7	20	4	40	20	190	10	11	ran pump briefly, picture
3/17/2005	8	17	4	40	20	180	12	13	waited approx. 45min
3/17/2005	9	17	4	40	20	180	14	15	no wait
3/17/2005	10	17	4	40	20	180	16	17	no wait
3/17/2005	11	17	4	40	20	180	18	19	no wait
3/17/2005	12	17	4	40	20	180	20	21	ran pump 10 min, saw arc begin to form off to side and corrected to electrode, bubbles
5/11/2005	13	20	4	40	20	90			pumped 20 min before, change to bandwidth limited, Ch.1 20 dB driven by 50 Ω

5/11/2005	14	20	4	40	20	190			shortened Ch. 2 cable after seeing reflections
5/11/2005	15	20	4	40	20	190			
5/12/2005	16	20	4	40	20	190	post1	pre1	pump ran day before at sat all night, multichanneling to electrode and gnd, 20 dB, 50Ω on both Ch.1,2
5/12/2005	17	20	4	40	20	190	post2	pre2	pump 37 minutes, stopped scope from averaging, change to 200ns, tried to take digital picture but blurred
5/12/2005	18	20	4	40	20	190	post3	pre3	no pump, bad pic, change to 400ns
5/12/2005	19	20	4	40	20	190	post4	pre4	pump 13 minutes, TG pre-fired, change scope to 20 MHz bandwidth limited
5/12/2005	20	20	4	40	20	190	post5	pre5	pump 20 min, increase SF6 in TG to 22 psi, no file
5/12/2005	21	20	4	40	20	190	post6	pre6	no pump, picture taken
5/12/2005	22	17	4	40	22	180	post7	pre7	
5/12/2005	23	17	4	40	22	180	post8	pre8	pump 40 min, no fire, possibly no - 40kV supply HV, one SG fire, purge SG SF 6
5/12/2005	24	17	4	40	22	180	post9	pre9	no pump, no data, scope triggered to early, sounded, looked like good shot
5/12/2005	25	17	4	40	22	180	post10	pre10	pump 5 min, no data, scope triggered to early, sounded, looked like bad shot
5/12/2005	26	17	4	40	22	180	post11	pre11	pump 10 min, sounded looked good, arc had legs but didn't touch gnd
5/12/2005	27	17	4	40	22	180	post12	pre12	pump 40 min, big time difference between charge and fire pulse on scope
5/12/2005	28	17	4	40	22	180	post13	pre13	no pump, wait 15 min, good shot, data
5/12/2005	29	20	4	40	22	180	post14	pre14	no pump, wait 20 min, bad shot
5/16/2005	30	20	4	40	22	180	post1	pre1	realigned electrodes by adjusting supports, pumped H2O out of oil 3 days, multichannel to electrode, gnd
5/16/2005	31	20	4	40	22	180	post2	pre2	pump 20 min, multichannel to electrode, gnd

5/16/2005	32	20	4	40	22	180	post3	pre3	pump 22 min, multichannel to electrode, gnd
5/16/2005	33	17	4	40	22	180	post4	pre4	pump 21 min, multichannel to electrode, gnd, pulse looked better
5/17/2005	34	32	15	60	40	90	post1	pre1	no pump, took bandwidth filtering off, overshoot scope so changed to 30 dB, observed billowy carbon clouds
5/17/2005	35	32	15	60	40	90	post2	pre2	pump 20 min, realigned with supports, pump 20 min, supports fell during shot, square pulse, lots carbon again
5/17/2005	36	32	15	60	40	90	post3	pre3	pump 30 min, fixed diagnostics with copper, realigned with cable
5/19/2005	37	32	15	60	40	190	post1	pre1	pump 45 min, multichannel to electrode, gnd
5/19/2005	38	32	15	60	22	240	post2	pre2	pump 30 min, multichannel to electrode, gnd, large carbon cloud
5/19/2005	39	17	6	40	22	180	post3	pre3	no fire, no data
5/19/2005	40	17	6	40	22	180	post4	pre4	no fire, no data, SG pressure too high
5/19/2005	41	17	4	40	22	180	post5	pre5	reduced SG pressure, good shot
5/19/2005	42	17	4	40	22	180	post6	pre6	no pump, multichannel to electrode only
5/19/2005	43	17	4	40	22	180	post7	pre7	thick arc to electrode only

APPENDIX E. MATLAB CODE

This MATLAB program accepts inputs for parameters for Abramyan network design. The program is based on the UMC Marx and prompts for the number of stages to reverse-charge from of the total number of stages in the Marx. The charge per stage is assumed to be 90 kV (+50 kV, - 40 kV) based on the current configuration of the Marx, but the program prompts for changes. The load impedance is assumed to be 300 Ω but the program again prompts for alterations. From these inputs, capacitance and inductance values are calculated for both the forward and reverse-charged stages. The inductor to be added to the Abramyan section is computed using the following equation.

$$L_d = \frac{V_a^2 \cdot R_L^2 \cdot C_e^2}{V_L^2 \cdot C_a} - L_a$$

Prior work used to derive the equation above is referenced in Chapter 6. Outputs from the program can be used for circuit simulation purposes.

```
clear;
format('short');

total_stages = input('Total number of stages in Marx: ');
reverse_stages = input('Total number of stages to reverse: ');
forward_stages = total_stages - reverse_stages;
charge_per_stage = input('Charge per stage: [90kV] ');
if isempty(charge_per_stage)
    charge_per_stage = 90000;
end
load = input('Load impedance: [300ohm] ');
if isempty(load)
    load = 300;
end

forward_voltage = charge_per_stage * forward_stages;
reverse_voltage = charge_per_stage * reverse_stages;
```

```

total_capacitance = inv(1/(48e-9)*(forward_stages +
reverse_stages));

load_voltage_beginning = 1.5e6;
load_voltage_end = 1e6;

Cm = inv(1/(48e-9)*(forward_stages))
V_Cm = forward_voltage
Lm = (4.6e-6/30 * forward_stages)

Ca = inv(1/(48e-9)*(reverse_stages))
V_Ca = -reverse_voltage
La = (4.6e-6/30 * reverse_stages)

Ld_sweep_beginning = (reverse_voltage * load * total_capacitance
/ load_voltage_beginning)^2 * (1/Ca) - La
Ld_sweep_end = (reverse_voltage * load * total_capacitance /
load_voltage_end)^2 * (1/Ca) - La

ApproxMarxOutput = V_Cm + V_Ca

```

Example of results:

```

Total number of stages in Marx: 22
Total number of stages to reverse: 5
Charge per stage: [90kV]
Load impedance: [300ohm]
Cm =
  2.8235e-009
V_Cm =
  1530000
Lm =
  2.6067e-006
Ca =
  9.6000e-009
V_Ca =
  -450000
La =
  7.6667e-007
Ld_sweep_beginning =
  3.2499e-006
Ld_sweep_end =
  8.2705e-006
ApproxMarxOutput =
  1080000

```


Total number of stages in Marx: 30
Total number of stages to reverse: 10
Charge per stage: [90kV]
Load impedance: [300ohm]
Cm =
2.4000e-009
V_Cm =
1800000
Lm =
3.0667e-006
Ca =
4.8000e-009
V_Ca =
-900000
La =
1.5333e-006
Ld_sweep_beginning =
1.5747e-005
Ld_sweep_end =
3.7347e-005
ApproxMarxOutput =
900000

Total number of stages in Marx: 20
Total number of stages to reverse: 3
Charge per stage: [90kV]
Load impedance: [300ohm]
Cm =
2.8235e-009
V_Cm =
1530000
Lm =
2.6067e-006
Ca =
1.6000e-008
V_Ca =
-270000
La =
4.6000e-007
Ld_sweep_beginning =
5.8976e-007
Ld_sweep_end =
1.9020e-006
ApproxMarxOutput =
1260000

Total number of stages in Marx: 25
Total number of stages to reverse: 7
Charge per stage: [90kV]
Load impedance: [300ohm]
Cm =
 2.6667e-009
V_Cm =
 1620000
Lm =
 2.7600e-006
Ca =
 6.8571e-009
V_Ca =
 -630000
La =
 1.0733e-006
Ld_sweep_beginning =
 7.4616e-006
Ld_sweep_end =
 1.8130e-005
ApproxMarxOutput =
 990000

APPENDIX F. MATHEMATICA CODE

This code was developed to solve the Laplace transform of the Marx and Abramyan circuit. Two current loops in the Marx-Abramyan circuit were developed and solved accordingly. Both the output voltage and ringing Abramyan voltage are plotted. Also, all signal components that combine to form the output pulse are shown in an additional plot. Values were used in place of variables due to extended computation time.

```

Clear[I1, I2, Ca, Va, La, Ld, Cm, Vm, Lm, R, s, V6, num, den, f6];
Solve[{{(1/(s*Ca)*I1) - (Va/s) + (s*La*I1) + (s*Ld*(I1 - I2)) == 0,
  (1/(s*Cm)*I2) - (Vm/s) + (s*Lm*I2) + (R*I2) + (s*Ld*(I2 - I1)) == 0}, {I1, I2}]
{{I1 -> -Vm/(Ld*s^2) - (R + 1/Cms + Ld*s + Lm*s) * (Ld*Va + ((1/Cas + Las + Lds)/s)*Vm) /
  (Ld*s*(Ld^2*s^2 - (1/Cas + Las + Lds)*(R + 1/Cms + Ld*s + Lm*s))},
  I2 -> - (Ld*Va + ((1/Cas + Las + Lds)/s)*Vm) /
  (Ld^2*s^2 - (1/Cas + Las + Lds)*(R + 1/Cms + Ld*s + Lm*s))}}
I2 = - (Ld*Va + ((1/Cas + Las + Lds)/s)*Vm) /
  (Ld^2*s^2 - (1/Cas + Las + Lds)*(R + 1/Cms + Ld*s + Lm*s));
Vm = 1.53*10^6;
Cm = 2.8*10^-9;
Lm = 2.6*10^-6;
Va = -450*10^3;
Ca = 9.6*10^-9;
La = 766.7*10^-9;
Ld = 5*10^-6;
R = 300;
V6 = I2*R
num = Collect[Numerator[V6], s]
numroots = Solve[num == 0, s]
den = Collect[Denominator[V6], s]
denroots = Solve[den == 0, s]

```

$$\frac{300 \left(-\frac{9}{4} + \frac{1.53 \times 10^6 \left(\frac{1.04167 \times 10^8}{s} + 5.7667 \times 10^{-6} s \right)}{s} \right)}{- \left(\frac{1.04167 \times 10^8}{s} + 5.7667 \times 10^{-6} s \right) \left(300 + \frac{3.57143 \times 10^8}{s} + 7.6 \times 10^{-6} s \right) + \frac{s^2}{4000000000}}$$

$$-1971.92 - \frac{4.78125 \times 10^{16}}{s^2}$$

{s → 0. - 4.9241 × 10⁶ i}, {s → 0. + 4.9241 × 10⁶ i}

$$-2851.2 - \frac{3.72024 \times 10^{16}}{s^2} - \frac{3.125 \times 10^{10}}{s} - 0.00173001 s - 1.88269 \times 10^{-11} s^2$$

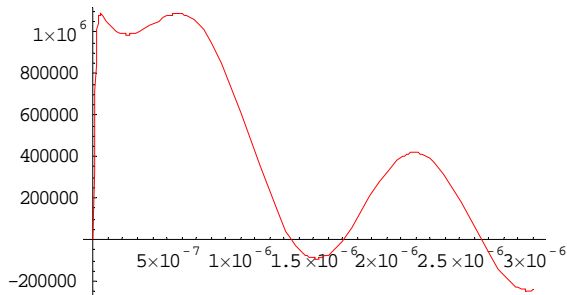
{s → -9.04156 × 10⁷}, {s → -1.22694 × 10⁶}, {s → -123828. - 4.21867 × 10⁶ i}, {s → -123828. + 4.21867 × 10⁶ i}

f6 = Simplify[InverseLaplaceTransform[V6, s, t]]

Expand[LaplaceTransform[InverseLaplaceTransform[V6, s, t], t, s]]

Plot[f6, {t, 0, 3 * 10^-6}, PlotStyle → {RGBColor[1, 0, 0]}]

$$\begin{aligned} & (-1.1785 \times 10^6 + 0. i) e^{-9.04156 \times 10^7 t} + (1.59052 \times 10^6 + 0. i) e^{-1.22694 \times 10^6 t} - \\ & (206009. - 10070.5 i) e^{(-123828. - 4.21867 \times 10^6 i) t} - (206009. + 10070.5 i) e^{(-123828. + 4.21867 \times 10^6 i) t} \\ & - \frac{206009. + 10070.5 i}{(123828. - 4.21867 \times 10^6 i) + s} - \frac{206009. - 10070.5 i}{(123828. + 4.21867 \times 10^6 i) + s} + \frac{1.59052 \times 10^6 + 0. i}{1.22694 \times 10^6 + s} - \frac{1.1785 \times 10^6 + 0. i}{9.04156 \times 10^7 + s} \end{aligned}$$



- Graphics -

a1 = -9.041563404309268`7;**

a2 = -1.2269389967064043`6;**

aratio = a1 / a2

c1 = -1.1784976473604566`6;**

c2 = 1.5905157613165756`6;**

Cratio = c1 / c2

73.692

-0.740953

```

sinfunc = ExpToTrig[-(206009.05697805953` - 10070.534283799661` i) e(-123828.2413040823` - 4.218669197291801`*i) t -
(206009.05697805953` + 10070.534283799661` i) e(-123828.2413040823` + 4.218669197291801`*i) t]

```

```

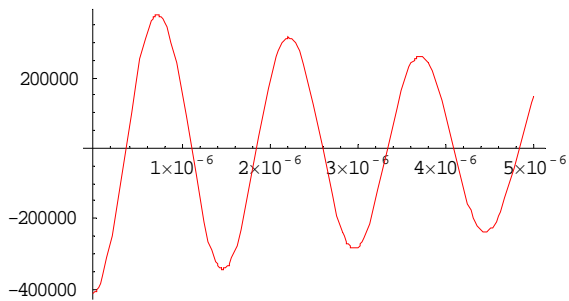
Plot[sinfunc, {t, 0, 5*10^-6}, PlotStyle -> {RGBColor[1, 0, 0]}]

```

```

(-206009. - 10070.5 i) Cos[(4.21867*10^6 + 123828. i) t] - (206009. - 10070.5 i) Cosh[(123828. + 4.21867*10^6 i) t] +
(10070.5 - 206009. i) Sin[(4.21867*10^6 + 123828. i) t] + (206009. - 10070.5 i) Sinh[(123828. + 4.21867*10^6 i) t]

```



- Graphics -

```

ftime1 = C1 * Exp[a1 * t];

```

```

ftime2 = C2 * Exp[a2 * t];

```

```

ftime3 = ftime1 + ftime2 + sinfunc

```

```

Plot[{ftime1, ftime2, sinfunc, ftime3}, {t, 0, 3*10^-6},

```

```

PlotStyle -> {RGBColor[1, 0, 0], RGBColor[0, 1, 0], RGBColor[0, 0, 1], RGBColor[1, 0, 1]}, AspectRatio -> 1,

```

```

PlotRange -> {-2*10^6, 2*10^6}]

```

```

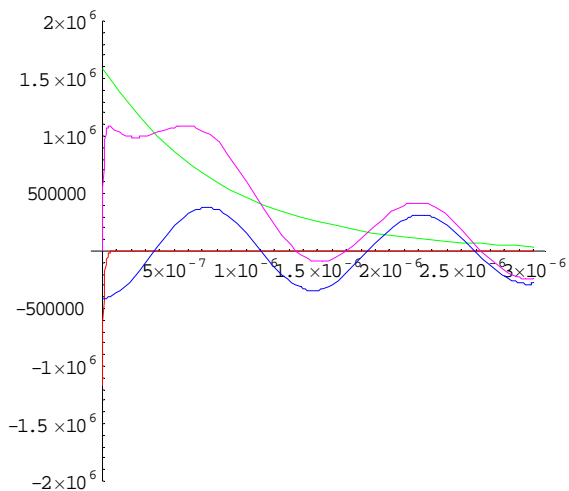
-1.1785*10^6 e-9.04156*10^7 t + 1.59052*10^6 e-1.22694*10^6 t -

```

```

(206009. + 10070.5 i) Cos[(4.21867*10^6 + 123828. i) t] - (206009. - 10070.5 i) Cosh[(123828. + 4.21867*10^6 i) t] +
(10070.5 - 206009. i) Sin[(4.21867*10^6 + 123828. i) t] + (206009. - 10070.5 i) Sinh[(123828. + 4.21867*10^6 i) t]

```



- Graphics -

APPENDIX G. ABRAMYAN SIMULATION CODE

This code was developed from PSPICE schematics to simulate the Marx parameters with the inclusion of the Abramyan network designed by the programs discussed in Appendix E and Appendix F. The program was instructed to compute a range of multi-variable parameters with varying inductor values. Results from these simulations are discussed in Chapter 6.

```
*Libraries:
* Local Libraries :
* From [PSPICE NETLIST] section of pspice91.ini file:
.lib "nom.lib"

*Analysis directives:
.TRAN 0 3us 0
.STEP LIN PARAM L 1uH 9uH 2uH
.PROBE N([N00467])
.INC "abramyan0601-SCHEMATIC1.net "

**** INCLUDING abramyan0601-SCHEMATIC1.net ****
* source ABRAMYAN0601
C_Cm          N00465 N00180  2.8nF IC=1.53MEGV
R_Rload       N00467 0  300ohm
L_Lm          N01367 N00467  2.6uH
R_Rd          N03766 0  1ohm
C_Ca          N05437 0  9.6nF IC=-450kV
X_U1          N05344 N00180 Sw_tClose PARAMS: tClose=0 ttran=1n
Rclosed=0.01
+ Ropen=1Meg
R_R1          N05424 N05344  1ohm
X_U2          N00465 N01367 Sw_tClose PARAMS: tClose=0 ttran=1n
Rclosed=0.01
+ Ropen=1Meg
L_La          N05437 N05424  766.7nH
L_Ld          N00180 N03766  {L}
.PARAM  L=1uH

**** RESUMING abramyan0601-schematic1-abramyan22stage.sim.cir
****
```

.INC "abramyan0601-SCHEMATIC1.als"

**** INCLUDING abramyan0601-SCHEMATIC1.als ****

.ALIASES

C_Cm Cm(1=N00465 2=N00180)
R_Rload Rload(1=N00467 2=0)
L_Lm Lm(1=N01367 2=N00467)
R_Rd Rd(1=N03766 2=0)
C_Ca Ca(1=N05437 2=0)
X_U1 U1(1=N05344 2=N00180)
R_R1 R1(1=N05424 2=N05344)
X_U2 U2(1=N00465 2=N01367)
L_La La(1=N05437 2=N05424)
L_Ld Ld(1=N00180 2=N03766)

.ENDALIASES

**** RESUMING abramyan0601-schematic1-abramyan22stage.sim.cir

.END

**** Voltage Controlled Switch MODEL PARAMETERS

.....

	X_U1.Smod	X_U2.Smod
RON	.01	.01
ROFF	1.000000E+06	1.000000E+06
VON	1	1
VOFF	0	0

**** INITIAL TRANSIENT SOLUTION

TEMPERATURE = 27.000 DEG C

**** CURRENT STEP PARAM L = 1.0000E-06

NODE	VOLTAGE	NODE	VOLTAGE	NODE	VOLTAGE	NODE	VOLTAGE
------	---------	------	---------	------	---------	------	---------

(N00180)	-1.9795	(N00465)	1.530E+06	(N00467)	458.8600		
(N01367)	458.8600						

(N03766)	-1.9795	(N05344)	-450.0E+03	(N05424)	-450.0E+03		
(N05437)	-450.0E+03						

(X_U1.3)	0.0000	(X_U2.3)	0.0000				
----------	--------	----------	--------	--	--	--	--

VOLTAGE SOURCE CURRENTS

NAME	CURRENT
X_U1.V1	0.000E+00
X_U2.V1	0.000E+00

TOTAL POWER DISSIPATION 0.00E+00 WATTS

**** INITIAL TRANSIENT SOLUTION
TEMPERATURE = 27.000 DEG C

**** CURRENT STEP PARAM L = 3.0000E-06

NODE VOLTAGE	NODE VOLTAGE	NODE VOLTAGE	NODE VOLTAGE
--------------	--------------	--------------	--------------

(N00180) -1.9795	(N00465) 1.530E+06	(N00467) 458.8600
(N01367) 458.8600		

(N03766) -1.9795	(N05344) -450.0E+03	(N05424) -450.0E+03
(N05437) -450.0E+03		

(X_U1.3) 0.0000	(X_U2.3) 0.0000
-----------------	-----------------

VOLTAGE SOURCE CURRENTS

NAME	CURRENT
X_U1.V1	0.000E+00
X_U2.V1	0.000E+00

TOTAL POWER DISSIPATION 0.00E+00 WATTS

**** INITIAL TRANSIENT SOLUTION
TEMPERATURE = 27.000 DEG C

**** CURRENT STEP PARAM L = 5.0000E-06

NODE VOLTAGE	NODE VOLTAGE	NODE VOLTAGE	NODE VOLTAGE
--------------	--------------	--------------	--------------

(N00180) -1.9795	(N00465) 1.530E+06	(N00467) 458.8600
(N01367) 458.8600		

(N03766) -1.9795 (N05344)-450.0E+03 (N05424)-450.0E+03
(N05437)-450.0E+03

(X_U1.3) 0.0000 (X_U2.3) 0.0000

VOLTAGE SOURCE CURRENTS
NAME CURRENT

X_U1.V1 0.000E+00
X_U2.V1 0.000E+00

TOTAL POWER DISSIPATION 0.00E+00 WATTS

**** INITIAL TRANSIENT SOLUTION
TEMPERATURE = 27.000 DEG C

**** CURRENT STEP PARAM L = 7.0000E-06

NODE VOLTAGE NODE VOLTAGE NODE VOLTAGE NODE
VOLTAGE

(N00180) -1.9795 (N00465) 1.530E+06 (N00467) 458.8600
(N01367) 458.8600

(N03766) -1.9795 (N05344)-450.0E+03 (N05424)-450.0E+03
(N05437)-450.0E+03

(X_U1.3) 0.0000 (X_U2.3) 0.0000

VOLTAGE SOURCE CURRENTS
NAME CURRENT

X_U1.V1 0.000E+00
X_U2.V1 0.000E+00

TOTAL POWER DISSIPATION 0.00E+00 WATTS

**** INITIAL TRANSIENT SOLUTION
TEMPERATURE = 27.000 DEG C

**** CURRENT STEP PARAM L = 9.0000E-06

NODE	VOLTAGE	NODE	VOLTAGE	NODE	VOLTAGE	NODE
------	---------	------	---------	------	---------	------

(N00180)	-1.9795	(N00465)	1.530E+06	(N00467)	458.8600	
(N01367)	458.8600					

(N03766)	-1.9795	(N05344)	-450.0E+03	(N05424)	-450.0E+03	
(N05437)	-450.0E+03					

(X_U1.3)	0.0000	(X_U2.3)	0.0000			
----------	--------	----------	--------	--	--	--

VOLTAGE SOURCE CURRENTS

NAME	CURRENT
X_U1.V1	0.000E+00
X_U2.V1	0.000E+00

TOTAL POWER DISSIPATION 0.00E+00 WATTS

JOB CONCLUDED

TOTAL JOB TIME .11